FUNCTIONALIZED CELLULOSE-BASED ADSORBENT FOR LITHIUM RECOVERY FROM AQUEOUS SOLUTIONS

A Thesis Submitted to
the Graduate School of Engineering and Sciences of
İzmir Institute of Technology
in Partial Fulfillment of the Requirements for the Degree of

MASTER OF SCIENCE

in Chemical Engineering

by
Jackline NAMPEERA

November 2021
İZMİR

ACKNOWLEDGMENTS

ABSTRACT

FUNCTIONALIZED CELLULOSE-BASED ADSORBENT FOR LITHIUM RECOVERY FROM AQUEOUS SOLUTIONS

This study focused on generation of low-cost yet highly effective lithium selective bio-sorbent from olive pruning waste mainly olive branches. Olive branches were treated with NaOH that eliminated non-cellulosic materials and activated hydroxyl groups that inhibit the formation of active sites. Olive branches were then functionalized through homogeneous phosphorylation at 150 ⁰C. POB, NOB, and FOB samples were subjected to SEM, XRD, FTIR, BET, XPS, and TGA to observe the changes in their structure and properties.

Factors affecting lithium adsorption were investigated on the synthesized FOB in a batch system and analyzed by ICP-OES. Adsorption isotherms are well fitted to the Freundlich isotherm model than the Langmuir isotherm model which exhibited a maximum adsorption capacity of 6.7 mg/g at 30 ⁰C. Kinetic studies exhibited fast kinetics and equilibrium was attained in 6 minutes while thermodynamic studies showed an exothermic, spontaneous reaction and increased randomness at the interaction interface. Regeneration studies proved the sustainability of FOB with Li^+ desorption efficiency of 99.6% in 1.0 M HCl. The synthesized FOB displayed a better degree of column utilization and elution efficiency; 56.8% and 95.8% than Lewatit TP 260; 16.0% and 50.4% respectively in the adsorption column studies performed at room temperature. However, it exhibited a poor breakthrough capacity of 2.1 mg Li/ml sorbent than Lewatit TP 260 with 1.33 mg Li/ml sorbent. Based on all experimental results, the novel functionalized olive branches (FOB) proved a potential lithium selective bio-sorbent and can be applied in recovery of lithium from its aqueous sources.

ÖZET

SULU ÇÖZELTİLERDEN LİTYUM GERİ KAZANIMI İÇİN FONKSİYONELLEŞTİRİLMİŞ SELÜLOZ BAZLI ADSORBENT

Bu çalışma, başta zeytin dalları olmak üzere zeytin budama atıklarından düşük maliyetli ancak oldukça etkili lityum seçimli biyo-sorbent üretimine odaklanmıştır. Zeytin dalları, selülozik olmayan malzemeleri ve aktif bölgelerin oluşumunu engelleyen aktif hidroksil gruplarını elimine etmek içim NaOH ile muamele edilmiştir. Zeytin dalları daha sonra 150 ⁰C'de homojen fosforilasyon ile aktifleştirildi. POB, NOB ve FOB örneklerinin, yapılarındaki ve özelliklerindeki değişiklikleri gözlemlemek için SEM, XRD, FTIR, BET, XPS ve TGA analizleri yapılmıştır.

Lityum adsorpsiyonunu etkileyen faktörler, bir kesikli sistemde sentezlenen FOB varlığında araştırılmıştır ve ICP-OES ile analiz edilmiştir. Adsorpsiyon izotermleri, 30 ⁰C'de 6,7 mg/g maksimum adsorpsiyon kapasitesi göstermiş ve Langmuir izoterm modelinden daha iyi Freundlich izoterm modeline uymuştur. Kinetik çalışmalar hızlı kinetik sergilemiş ve dengeye 6 dakikada ulaşılırken, termodinamik çalışmalar etkileşim arayüzünde ekzotermik, kendiliğinden bir reaksiyon ve artan rastgelelik göstermiştir. Rejenerasyon çalışmaları, 1.0 M HCl'de %99.6'lık Li+ desorpsiyon verimliliği ile FOB'un sürdürülebilirliğini kanıtlamıştır. Sentezlenen FOB, Lewatit TP 260'a göre daha iyi derecede kolon kullanımı ve elüsyon verimliliği göstermiştir; oda sıcaklığında gerçekleştirilen adsorpsiyon kolonu çalışmalarında FOB ve Lewatit TP 260'ın kolon kullanımı ve elüsyon verimliliğ sırasıyla %56,8 ve %95,8; %16,0 ve %50,4 olarak belirlenmiştir. Fakat, Lewatit TP 260, 1,33 mg Li/ml geçiş kapasitesi gösterirken FOB, 2,1 mg Li/ml ile zayıf bir geçiş kapasitesi göstermiştir. Tüm deneysel sonuçlara dayanarak, yeni işlevselleştirilmiş zeytin dallarının (FOB), potansiyel bir lityum seçimli biyo-sorbent olduğu kanıtlanmıştır ve lityumun sulu kaynaklarından geri kazanımında kullanılabilir.

TABLE OF CONTENTS

APPENDICES

LIST OF FIGURES

LIST OF TABLES

LIST OF ABBREVIATIONS

AC	Activated Carbon
q_e	Adsorbed lithium amount at equilibrium (mg/g)
BET	Brunauer–Emmett–Teller
CGG	CMS grafted with glycidyl methacrylate
DMF	Dimethylformamide
EPI	Epichlorohydrin
EDA	Ethane Diamine
FTIR	Fourier Transform Infrared Spectroscopy
FOB	Functionalized Olive Branches
ΔG^0	Gibbs free energy
GAC	Granular Activated Carbon
LiCGC™	$Li1+x+yAlx (Ti, Ge)_2-xSiyP_3-yO_{12}$
M_{ads}	Mass of adsorbent
q_{max}	Maximum adsorption capacity (mg/g)
MCC	Microcrystalline Cellulose
CMS	Microcrystalline Cellulose Microsphere
NOB	NaOH-treated Olive Branches
PAC	Powdered activated carbon
POB	Pristine Olive Branches
SEM	Scanning Electron Microscopy
NaClO	Sodium hypochlorite
ΔH^0	Standard enthalpy change
ΔS^0	Standard entropy change
CGS	Sulphonated/functionalized CMS/
TGA	Thermogravimetric Analysis
XRD	X-ray Diffraction

CHAPTER 1

INTRODUCTION

Lithium is the least dense metal and comparatively rare element but also the most demandable in industrial production of non-rechargeable devices e.g., heart pacemakers and rechargeable lithium batteries commonly used in electronics and electric cars. Additionally, lithium demand has dynamically hiked in recent years due to the tremendous development in other lithium-based technologies such as nuclear reactors, pharmaceuticals, Metallurgy, and glass and ceramics production (Battistel et al. 2020; Kavanagh et al. 2018)

Several metal ion extraction techniques such as solar evaporation (Cheng et al. 2019; Yu et al. 2021; Q. Zhang et al. 2021), electrodialysis (Jiang et al. 2014), solvent extraction (Shi et al. 2017; Zante et al. 2019), chemical precipitation (Um and Hirato 2014) and electrocoagulation (Nidheesh et al. 2020) have been studied to improve their cation extraction efficiency however still hindered by copious factors such as long production periods, high costs and more as discussed in Chapter 2. Adsorption is a popular technique in the treatment of water and extraction of lithium and other metals from their aqueous sources. Both organic and inorganic adsorbents generally have porous layered structures that enhance mass transfer and diffusion for a higher uptake of ions, mainly favored by low production costs and low cation concentrations in the aqueous sources (Babel and Kurniawan 2003; Khader et al. 2021; Paliulis 2016). Inorganic adsorbents e.g., lithium ion-sieve (LIS) and H_2TiO_3, lithium manganese oxides (LMOS) have a high lithium uptake capacity, superior selectivity for lithium and other metals, have a good cycle performance but possess a toxic chemical nature, sophisticated synthesis, quite costly and non-biodegradable as compared to organic adsorbents (X. Xu et al. 2016). On the contrary, organic adsorbents (bio sorbents) have gained a reputation in adsorption scientific research for the past few decades to provide sorbents with high efficacy at low cost as an alternative.

These are obtained from several biomasses with a high cellulose content such as agricultural wastes i.e., cotton (Akpomie and Conradie 2020), rice husk (Samah et al, 2020), green coconut shells (Sousa et al. 2010), and agro-industrial wastes e.g., sugar bagasse (Sarker et al. 2017) and they a reputation for high efficacy on the removal of lithium and other metals from their sources, incur low production costs and readily available (Alkherraz, Ali, and Elsherif 2020; Ibrahim et al. 2017)

In this study, olive tree pruning waste mainly consisting of branches was selected as the biomass source of the organic adsorbent due to the abundance of olive trees in Turkey. It has been a major crop in the Mediterranean basin for 8000 years due to its health benefits, traditions, and most importantly economic growth contribution favored by the mild winters and summers. In 2019-20, total world virgin olive oil production was 3.2 million tonnes headed by Spain owning 35% followed by Italy, Tunisia, Greece, and Turkey (7.2%) respectively (IOC, 2021) This has caused an accumulation in olive pruning waste that is burnt causing environmental pollution in these olive growing regions (Fraga et al. 2021). This study focused on the utilization of these olive pruning wastes by converting them into a low-cost and environmentally friendly lithium selective bio sorbent through the attachment of phosphoric functional groups through the phosphorylation process. Based on the current literature, there is no study regarding the synthesis of lithium selective bio sorbents from either olive pruning waste or olive waste mainly composed of olive branches.

In this study, Pristine Olive Branches (POB), NaOH treated Olive Branches (NOB), and the Functionalized Olive Branches (FOB) - adsorbent synthesized from olive pruning waste mainly consisting of olive branches were characterized by SEM-EDX, FTIR, XRD, TGA, and BET to determine their structural changes and properties after modifications but more purposely to confirm the successful synthesis of the adsorbent. Lithium model solution (10 mg/L LiCl) was used to determine the efficacy of FOB adsorbent during pH, adsorbent dosage effect, initial concentration effect, and temperature effect investigations. The impact of contact time (kinetic studies) and thermodynamic properties were also evaluated. The effectiveness of lithium sorption and desorption on FOB adsorbent and a commercial lithium selective resin Lewatit TP 260 was compared through adsorption column studies. Lewatit TP 260 is a cation exchange resin with chelating aminomethyl phosphonic acid groups that particulate in the adsorption reactions. Also, no column adsorption studies on Lewatit TP 260 have been found in the current literature.

CHAPTER 2

LITERATURE REVIEW

2.1. Objectives and Importance of the Study

As stated in the introduction part of this thesis, the main aim of this study is to synthesize a cellulose-based adsorbent for lithium adsorption from its water resources, by eliminating the non-cellulosic components of olive branches (Olea europaea L. 'Oueslati') biomass through alkali treatment and then modifying its cellulose through the addition of a phosphoryl function group responsible for lithium selectivity. The other objectives are to study the structure and properties of the synthesized adsorbent and to investigate the factors affecting lithium adsorption on the adsorbent. Olive branches biomass was selected as the lithium adsorbent source in this study because of the abundance of olive trees in the Mediterranian regions especially Turkey. Turkey hold forth position in worldwide olive oil production contributing about 7.2 % as of 2020 (Fraga et al. 2021).

Lithium extraction has gained massive interest in the past two decades due to major developments and the use of lithium-ion batteries (35%), transportation, and communication industrial sectors as these consume the biggest percentage of lithium produced worldwide, headed by China with 39%.

2.2. Lithium sources

The primary lithium sources i.e., Pegmatites, and geothermal brine contain more than 1000 ppm Li. Other lithium-containing minerals are lepidolite, amblygonite, zinnwaldite, eucryptite, Jadar, and Petalite but currently, secondary sources are now eyed to meet the supply (Battistel et al, 2020). Geothermal waters worldwide contain between 1-100 ppm of Lithium and an average of 0.17 exists in seawater. The higher lithium concentration in geothermal water is mainly due to the leaching of the rocks in the aquafers aided by the higher water temperatures (Flexer, Baspineiro, and Galli 2018). And the growing interest in lithium extraction from water sources is attributed to

its natural abundance. Much of the extracted lithium is obtained from continental brines as these contain the largest resource for lithium in form of lithium carbonate at 59% (Battistel et al. 2020; Murodjon et al. 2020).

2.3. Major Applications of Lithium and Its Isotopes

Lithium was discovered in 1817 by Johan August from a mineral and this explains its name origin "Lithos" translated as stone in Greek. Lithium and its compounds have got a wide range of industrial applications in Lithium-Ion Batteries (LIB) and other sectors as discussed in this section, also summarised in Figure 1 and

Figure **2** respectively.

Electric mobility: Compared to standard hydrogen electrodes, lithium metal is now widely used in rechargeable batteries as an anode due to its low density 0.59 g cm^{-3}, the high specific capacity of 3860 mAh g^{-1}, and low negative electrochemical potential of 3.040 V (W. Xu et al. 2014). Lithium carbonate is majorly used in batteries for hybrid and electric vehicles, batteries for the grid, and in digitalization and communication devices such as phones, laptops, etc. All these are the future of the generations to come.

Nuclear energy production: Lithium is an excellent thermal conductor used in nuclear reactors as a heat transfer due to its high boiling temperature (1342 °C) (Oliviera et al. 2017). Its isotopes i.e., lithium-6 (7.59 %) and lithium 7 (92.41 %) of natural lithium have a major role in the production of thermonuclear energy production. lithium-7 isotope is used as a coolant in high-temperature reactors while lithium-6 is used as an absorber for thermal neutrons which when irradiated produces a tritium atom that is reacted with deuterium to produce fuel used in nuclear fusion reactors. This yields at least 17.6 MeV per reaction. Lithium-based ceramics i.e. (Li_2O, $LiAlO_2$, Li_2TiO_3, Li_2ZrO_3, and Li_4SiO_4) are used to produce tritium for blankets of fusion reactors.

Pharmaceuticals: Lithium carbonate is currently used in the treatment of bipolar disorder and patients with depression although its trigger on the brain is still fully not unknown (Oruch et al. 2014).

Glass and ceramics production: Lithium and its compounds are used as a temperature coolant in the production of glass, reduces thermal expansion and fluidities (elasticity) of the mixture, hence lowering production cost. In ceramics production, lithium oxide is used in lowering firing temperature, therefore, increasing strength in ceramic bodies. Lastly, lithium contributes to the longevity of cookware ceramics and

glasses by increasing their resistance to shock, mechanical strength above all, acts as an anti-corrosive element.

Metallurgical use: Lithium makes alloys with various metals, but aluminum and lead alloys are the most applicable ones. Al-Li alloy is very light and stable making it suitable for aircraft components while the Pb-Li alloy is used in bearings of railway wagons. Lastly, its chloride and bromide are used in air conditioning systems and industrial drying systems.
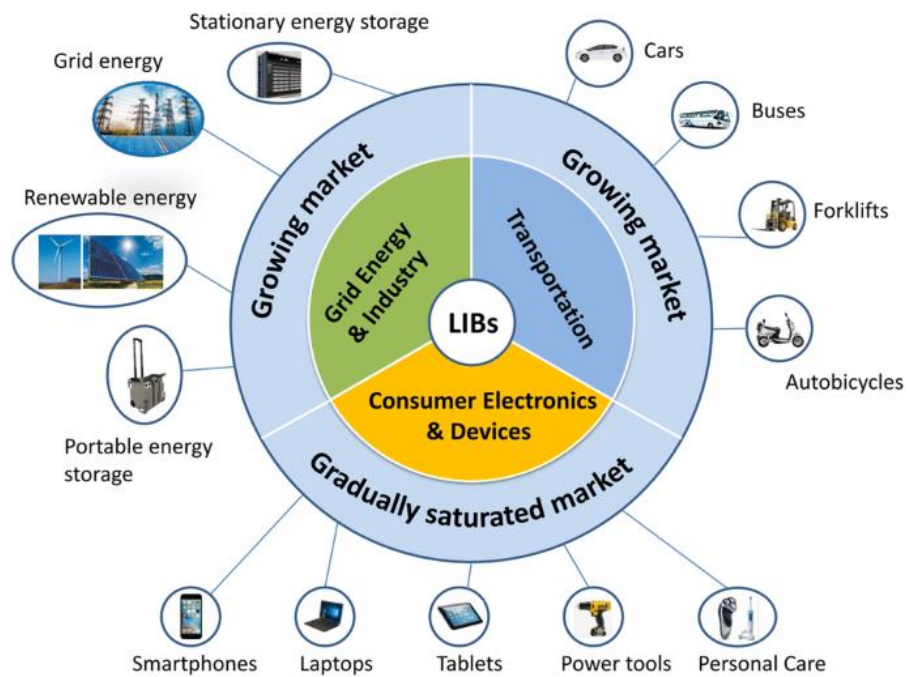
Figure 1. Major applications of Lithium-Ion Batteries

(Source: Ding et al. 2019)

LITHIUM DEPOSITS

Lithium minerals

Brines

PRIMARY PRODUCTS

Mineral concentrates

Lithium carbonate
Li$_2$CO$_3$

Lithium hydroxide
LiOH

Lithium chloride
LiCl

SECONDARY (DERIVED) PRODUCTS

Other lithium salts
acetate, benzoate,
phosphate …

Other lithium salts
stearate

Other lithium salts
nitrates, silicates,
sulphates …

Lithium bromide
LiBr

Metallic lithium
Li

Lithium zeolites

Other Li halogenides
LiClO$_4$, LiF, LiI ..

Butyllithiym

Other organic Li
compounds

USES AND APPLICATIONS
OF LITHIUM PRODUCTS

Lithium grease

Air
conditioning

Production of
elastomers

Catalysis
Air separation

Technical-grade products for:
• Glass and ceramics
• Steel continuous casting
• Aluminum melting

Battery-grade for:
• Li-ion batteries (secondary,
rechargeable, batteries)

High purity grade for:
• Pharmaceuticals

Technical-grade products for:
• CO2 scrubbing
• Steel continuous casting
• Aluminum melting

Battery-grade for:
• Primary (non rechargeable) lithium
batteries
• Li-ion batteries (secondary,
rechargeable, batteries)

*Numerous aplications
(examples):*
• Li-ion batteries (LiClO$_4$)
• Aluminum production (LiF)
• Nuclear physics (LiF)
• UV optics (LiF)
• Organic Light-Emitting Diodes
(OLED) (LiF)
• Long-life batteries in pacemakers
(LiI)
• High-temperature batteries (LiI)

• Al-Li alloy (aircraft
manufacturing)
• Primary batteries

• Glass and ceramics
• Steel continuous casting

LEGEND

Primary products
directly derived from
brine or minerals

Raw materials for
pharmaceuticals
and polymers production

Other important raw
materials

Main Li uses and
applications

Figure 2. Summary of applications lithium and its compounds

(Source: Christmann et al. 2015)

2.4. Lithium Market Projection

Lithium demand is projected to increase by roughly 60 % from 102,000 to 162,000 tonnes of lithium carbonate equivalent in the next decades, with battery applications taking a huge percentage of this growth (Murodjon, 2019). Lithium demand is expected to grow soon, at least up to 900 Ktons per year till 2025 (Battistel et al, 2020). A clear projection of lithium demand can be observed in Figure 3. It is, therefore, crucial to develop low-cost but yet effective lithium extraction techniques to meet this high lithium demand.

Figure 3. Lithium demand and supply Forecast 2015-2040.
(Source: (Investor, 2021)

2.5. Lithium Extraction and Recovery Methods

Since the rise of lithium demand in the 19th century, several technologies for lithium extraction from water have been developed but these are mainly affected by high costs, long time, and recovery efficiency Also, many lithium production techniques lack favorable processes for its separation, concentration, and purification due to its chemical

properties (Glaucia, 2017). These lithium extraction techniques are categorized into hydrometallurgy (mainly used in the leaching of lithium ores) and pyrometallurgy mainly used in lithium extraction from water sources. Figure 4 shows a general method for the extraction of lithium from its brines.

2.5.1. Evaporitic Technology

It is an ancient technology favored by an abundance of solar energy. Lithium ions in brines are concentrated by removal of other metal salts (of Li_2CO_3, NaCl, and Mg $(OH)_2$, $MgCO_3$) through crystallization or chemical precipitation. The obtained concentrated brine is then purified by removing metals e.g., boron, magnesium, and calcium (Epstein et al.,1980). The evaporation process is mainly affected by Mg/Li ratio, evaporation rate, ambient temperature, and impurity profile. This method increases lithium concentration from 2000 ppm to about 60,000 ppm in brines as they move from one pond to another.

Lalasari et al. 2020 studied the removal of lithium from brine water using the evaporation technique where brine was collected from Tirtasanita Bogor, Indonesia, and heated at different evaporation ratios to obtain prime water and salt deposit which was filtered and analyzed by ICP-OES. Results showed 17.27 ppm Li; 409.98 ppm K; 1929.87 ppm Na; 185.71 ppm Ca; 146.02 ppm Mg (Lalasari et al. 2020).
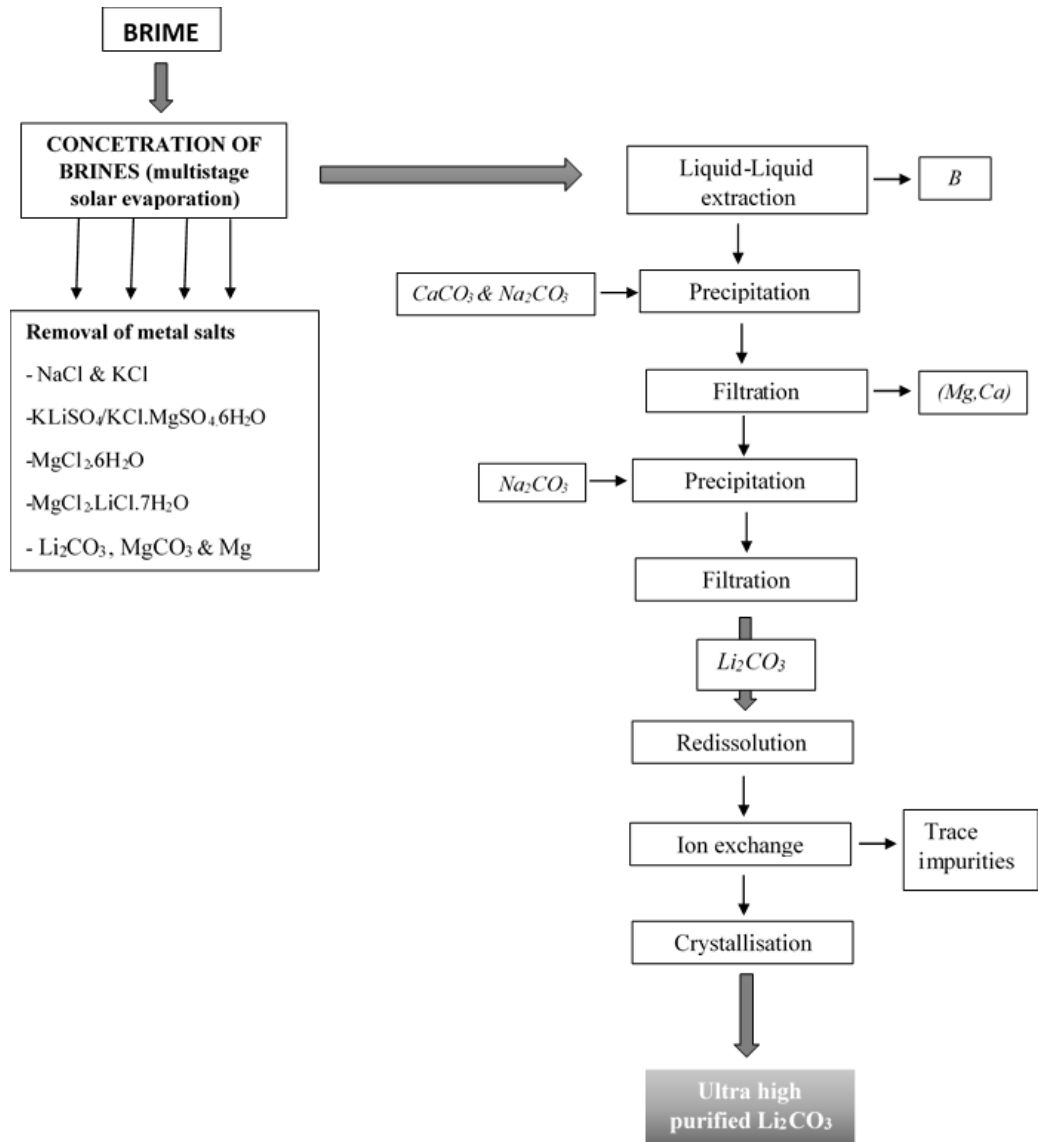
Figure 4. A combined process flow of lithium extraction techniques from brines

2.5.2. Electrodialysis (ED)

An electrical potential between the anode and cathode membranes as a driving force is used to separate ions from water sources as illustrated in Figure 5. Cations drift to the cathode while anions drift to the anode. Hoshino 2013 studied the recovery of lithium from seawater using electrolysis with membranes only selective to other competitive ions (Mg, Ca, Na, K) except Li^+. This caused a higher concentration of Li on the anode side, collected and analyzed. To increase the membrane efficiency, Mg^{2+} and Ca^{2+} concentrated seawater was then added to the anode, and ion-free seawater was

added to the cathode. This increased Li extraction efficiency from 38 % to 63 % using SELEMION$^{(TM)}$ membrane. (Gmar and Chagnes 2019) Nafion was used to increased membrane lifespan, Selemion™ AMV was used as an anionic membrane, The cationic membranes were impregnated with N-methyl-N-propylpiperidium-bis-(trifluoro methane-sulfonyl) imide (ionic liquid) to fasten transportation. In this study, Li recovery was increased from 5.9 to 22.2 % (Hoshino 2013)
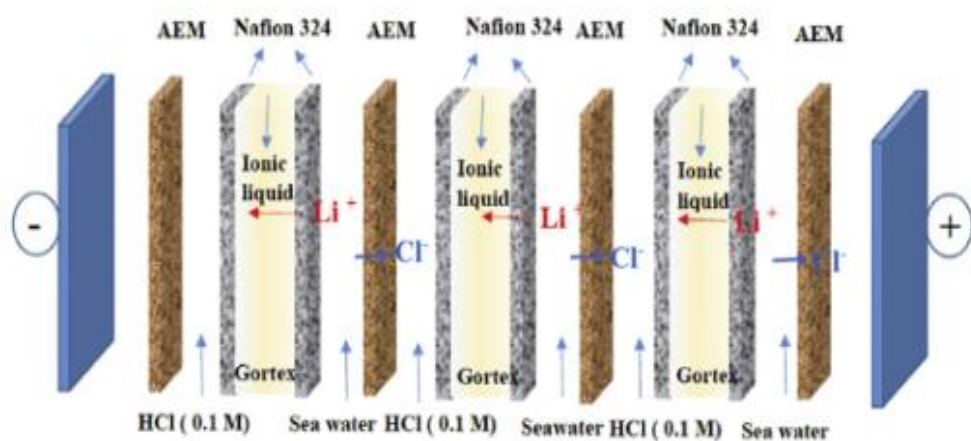
Figure 5. A set up for lithium extraction from seawater by electrodialysis (Gmar and Chagnes 2019)

Fauvarque and Lepinasse obtained a lithium recovery of 95% by grafting Diazo [2,2,2] bicyclo octane (DABCO) onto Poly epichlorohydrin. Boron nitride was added to increase chemical resistance and DABCO was partially replaced by sulfonated amine-poly- (ether sulfone). 47.8% of LiCGC in the membrane was used to increase Li conductivity. (Fauvarque and Lepinasse, 2018).

2.5.3. Solvent Extraction

This technique separates compounds or metals complexes based on their relative solubilities using chemical potential as a driving force. The two immiscible liquids the diluent and the extractant usually with an acidic PH are bought into contact. The

chemical potential drives the net transfer of species into another phase until equilibrium has been reached to create an extract and raffinate. (Schmidt et al. 2019). A special chelating agent, dipivaloyl methane is commonly used for the recovery of lithium from the aqueous solutions with low amounts of lithium (Nguyen and Lee 2018).

Lithium extraction methods have currently been further studied and developed to meet the equilibrium of the demand and supply curve of the lithium market as shown in Table 1. The advantages and disadvantages of these extraction methods are outlined in Table 2.

Table 1. Lithium recovery studies from respective sources
(Source: Murodjon et al. 2020)

Source	Process	Reagent	Product (purity %)	References
Brine	Ion exchange	MC50 resin, TP207 resin and Y80-N Chemie AG	LiCl solution	Bukowsky, Uhlemann, and Steinborn 1991
Salt Lake brine	Ion exchange	Synthesized H_2TiO_3	Li salt solution (97%)	Chitrakar et al. 2014
Seawater	Integrated ion-exchange method	λ -MnO_2	Li_2CO_3	Nishihama, Onishi, and Yoshizuka 2011
Brine	Liquid liquid extraction	2-ethyl 1,3 - hexanediol and isoamy alcohol	LiCl solution (90%)	Bukowsky and Uhlemann 1993
Brine	Liquid liquid extraction	Tri butayl phosphate	LiCl solution	Z. Zhou et al. 2012
Alkaline Brine	Liquid liquid extraction	Beta-diketone and trioctylphosphine oxide	LiCl solution (99%)	Wang et al. 2018

Cont. on next page

Table 1 (cont.)

Salt Lake Brine	Ionic Liquid-liquid extraction	Tri iso butyl phosphate in ionic liquid and kerosene	Li solution	Gao et al. 2015
Seawater	Adsorption	Nano structure MnO_2 ionseive	Li solution	(Zandevakili, Ranjbar, and Ehteshamzadeh 2014)
Seawater	Adsorption	MnO_2	Li solution	Liu et al. 2015
Brine	Adsorption	$Al(OH)_3$	Li salt solution	Hawash et al. 2010
Brine	Chromatography	Polyacrymide gel, Bio Gel P-2, and Blue Dextran 2000	LiCl solution	Rona and Schmuckler 1973
Subsurface Brines	Chromatography	Dionex CG-2 column	LiCl solution	Singh and Abbas 1996

Despite the available extraction techniques, lithium extraction from water sources is still relatively costly due to its trace existence and adsorption is currently the most suitable for recovery of metals from the diluted aqueous solutions (Kitajou et al. 2003; Ince and Ince 2017) revealed that adsorbents have high metal ion removal capabilities from diluted water sources.

Table 2. Advantages and disadvantages of common lithium extraction techniques

Lithium extraction method	Reference	Advantages	Challenges
Solar evaporation	(Wietelmann et al.,2014). (Flexer, Baspineiro, and Galli 2018)	• Concentrates big volumes of lithium solutions. • economically feasible and environmentally friendly.	• An extremely slow process as it requires 1-2years • Lower evaporation efficiency due to loss of heat to the surroundings. • Requires large evaporation areas or ponds. • A weather dependent process
Electrodialysis	(Strathmann, 2004) (Gmar and Chagnes 2019)	• Best at removing low molecular weight ionic components from a feed stream • Higher feed recovery is attainable.	• Favors higher lithium concentrated solution • Ions with low mobility capacity are not favored. • Requires keeping feed concentration higher as this maintains the driving force.

Table 2 (cont.)

Liquid-liquid extraction	Sonoda et al.,2014) (Swain, 2016)	• Simple and cheap • Good for small scale • High efficiency	• Long extraction time. • Uses large solvent volume • Process is energy intensive
Chemical Precipitation	(Nguyen et al., 2018).	• Favored by low calcium and magnesium concentrated brines.	• Gives lower quality products due to the slow kinetics and co-precipitation of other metals in the solution. • Requires large amounts of chemicals.
Adsorption	(Ince and Ince 2017)	• High rate of separation and recovery efficiency • Environmentally and economically friendly. • Adsorbents are easy to synthesize, regenerated and reused. • Adsorbent sources are obtainable	• Favors solutions with low ion concentration. • Some material is lost during the washing step

2.5.4. Lithium Extraction from Used Libs

Currently, used lithium-Ion batteries (LIB) are used as a secondary source for lithium as summarized in Figure 6. Used LIBs are collected, dismantled and their main components are categorized i.e., anodes, cathodes, casings, electrolyte, and current conductors (Al and Cu). The lithium oxide cathode of batteries i.e., Lithium Cobolt Oxide (LiCoO), lithium nickel dioxide (LiNiO2), and lithium manganese (III, IV) oxide (LiMn2O4) are the main sources of lithium during this process. Lithium is leached out and later extracted by precipitation in form of LiOH or Li_2CO_3 (Li et al. 2018; Castillo et al. 2002).

Nayaka et al. 2015 recovered lithium from ion batteries using dissolving LIB $LiCoO_2$ cathode material in a mixture of citric acid (chelating agent) and ascorbic acid (reductant) at 80 °C at dissolution rate constants (k) of 3.1×10^{-3} min^{-1} for Li and 0.8×10^{-3} min^{-1} for Co ions. Lithium and cobalt and were selectively precipitated as LiF and Co-oxalate and using oxalic acid and NH4F, respectively. Complete removal of Li was reported however the capacity was not reported (Nayaka et al. 2015).
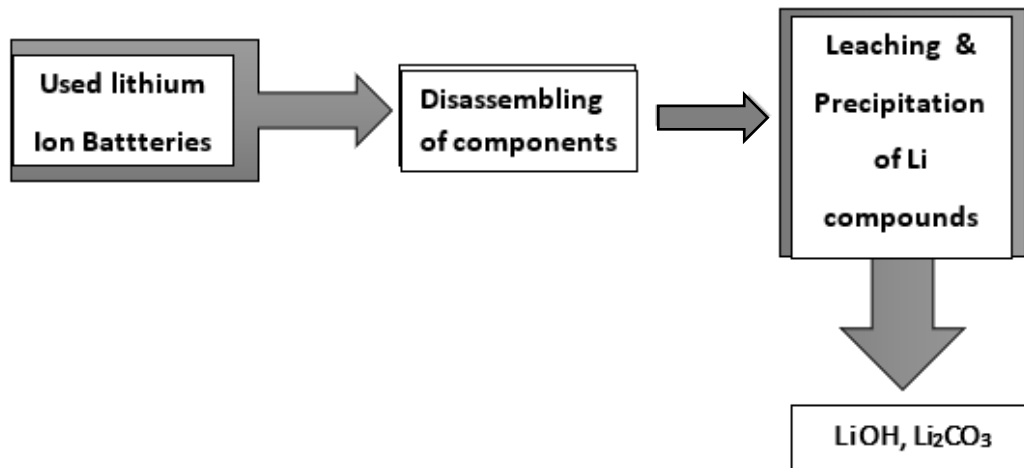
Figure 6. Process flow of lithium extraction from used Lithium-Ion Batteries.

(Pinna et al. 2017)

2.5.5. Adsorption

In the adsorption technique, lithium ions are selectively separated from their aqueous sources via physical or chemical adsorption. The adsorption method has been recognized as one of the most suitable technologies for the recovery of lithium from aqueous resources especially with low concentration, also both organic or inorganic adsorbents can be filtered after the adsorption process and recycled for reuse (Willy et al., 2016; Y. Zhang et al., 2020). Adsorbents can be generated from natural sources or directly chemically synthesized for commercial use (Chitrakar et al. 2001; Hameed, Fahad, and Ali 2017), and based on the literature, lithium-ion extraction from water by adsorption has proved satisfactory in terms of recovery efficiency (Q. X. Liu et al. 2019; Y. Zhou and Zhang 2016; Zhao et al. 2020).

2.5.5.1. Adsorbent Types

Various adsorbents have so far been synthesized from biomass sources (organic adsorbents) or directly chemically synthesized (inorganic adsorbents). However the latter incur high costs and are environmentally non-friendly and this has been addressed in this study, to synthesize a better adsorbent than the latter. Organic adsorbents are generally chemically modified to increase their adsorption capacity and efficiency (Schwantes et al. 2016).

2.5.5.2.   Inorganic Adsorbents

Inorganic adsorbents summarised in Table 3 have gained popularity due to their higher adsorption capacity as compared to most organic adsorbents, however these are limited by high costs and their potential dangers to the environment (Ayraktar 2007). Zhao et al. synthesized $Li_4Ti_5O_{12}$ by calcination process and then chemically modified it by reacting it with hydrochloric acid. The adsorbent attained a maximum lithium recovery of 90 %. Also, the $H_4Ti_5O_{12}$ nanorod reached a maximum adsorption capacity of 23.20 mg g^{-1} in 24 m LiCl solution in batch adsorption studies fitting Langmuir isotherm. Maximum lithium adsorption capacity reached 1.99 mmol g^{-1}, which was much higher

than 0.03 mmol g^{-1} and 0.02 mmol g^{-1} for magnesium and calcium respectively (Zhao et al. 2020).

In another study for lithium extraction from seawater using manganese oxide adsorbent synthesized from $H_{1.6} Mn_{1.6} O_4$, maximum lithium adsorption of 40 mg/g of adsorbent was reached. This study was limited using high temperatures in the synthesis of $H_{1.6} Mn_{1.6} O_4$, by heating $LiMnO_2$ at 400 °C to obtain other isotopes also studied in the same study (Chitrakar et al. 2001).

Zhong et al. worked with a novel-based nanocomposite biopolymer (EP-N+ -Zr) encapsulated with hydrous zirconium oxide to eliminated phosphate from aqueous solutions. The adsorbent was synthesized and modified by reacting 15g of $ZrOCl_2 \cdot 8H_2O$ within 100 mL of HCl (5 %, v/v) and alcohol (30 %, v/v) then, 5 g of EPN$^+$ -Zr was added and stirred for 12 h at 323 K. The result was filtered then mixed with 100 mL of 0.5 M of NaOH-NaCl each. The resulting mixture was continuously stirred at 293 K for 12 h to make the adsorbent Based on the characterization results the adsorbent had specific site structures that potentially increased its affinity for phosphate groups in the aqueous i.e., the embedded HZO nanoparticles and quaternary ammonia groups [N$^+$ (CH$_2$CH$_3$)$_3$Cl$^-$] bonded inside the biomass—Enteromorpha prolifera giving the adsorbent maximum adsorption of 88.5 mg(Phosphate)/g and well fitted with Langmuir isotherm (Zhong et al. 2021).

In the adsorption equilibria investigation of both granular and powder forms of manganese dioxide (λ-MnO2) derived from spinel-type lithium manganese dioxide, the granular adsorbent had an optimum amount of 6.0g/L of geothermal water while the powder adsorbent had 1.0g/L of geothermal water exhibiting a maximum adsorption capacity of 30.42 mg/L and 31.55mg/L (Recepoğlu et al. 2017).

Ryu et al. (2015) worked to enhance the adsorption capacity of porous cylinder type lithium manganese oxide by addition of sodium carbonate as an additive in a range of 2-10% by weight through acid treatment (0.3 M HCl) at 25°C. This increased the adsorbents maximum adsorption capacity of lithium from 15.06 mg/L to 19.9 mg/L with a 7% weight additive (Ryu et al., 2015)

Table 3. Comparison of inorganic lithium selective adsorbents

Adsorbent	Experimental conditions	Li source	Capacity (mg/g)	Reference
Polymeric porous microsphere adsorbents with crown ether	The initial concentration of 80 mg/L at PH 7. Equilibrium time of 20 min	Aqueous solution	2.31 mg/g	Yuan et al., 2019
Lithium manganese oxide precursor ($LiMn_2O_{4)}$ with ion sieves (λ-MnO_2)	PH= 9.19 at Equilibrium time of 102 hours at 293 K	LiCl solution	16.9 mg/g	Q. H. Zhang et al., 2007
Lithium manganese oxide precursor ($Li_{1.6}Mn_{1.6}O_4$) with ion sieves ($MnO_2 \cdot 0.5H_2O$)	The initial concentration of 0.17 mg/L and equilibrium was attained in two days.	Seawater	40.9 mg g^{-1}	Chitrakar et al., 2001
Functionalized titanate nanotubes	initial concentration 30 mg/L with PH 8 at 298K	Li$^+$ solution	40.26 mg/g	Kamran and Park 2020
Iron dropped Manganese oxides with an Ion-Sieve	NaOH-added brine (PH 8.2) Raw brine (PH 6.7) An adsorbent with a Fe/Mn	Raw brine and NaOH-added brine.	18 mg/g at final pH 2.0 from the raw brine And 28 mg/g at final PH 7.2 from	Chitrakar et al., 2014

Table 3 (cont.)

	ratio of 0.1. temp 450 °C		the NaOH-added brine.	
Li^+ adsorbent (H_2TiO_3)	Initial concentration 694.1 mg/L Li+	LiOH solution	39.8 mg/g	Shi et al., 2013
Natural and synthetic zeolites applying poly(acrylic acid)	Initial pH and concentration of geothermal water 5.5 and 10 mg/L	Geothermal water	0.5 mg/g synthetic Na-X zeolite with PAA and 5 mg/L in geothermal water clinoptilolite/PAA system	Wiśniewska et al., 2018
Ion dopped lithium titanium oxides (Obtained via Fe/Ti reaction with ratio 0.15 at 600°C + acid treatment)	Li concentration of 1.56 mg/L at PH 8.8 at room temperature for 55 hours.	Brine	34.8 mg/g	Wang et al., 2018
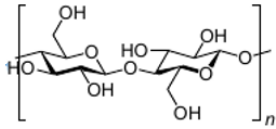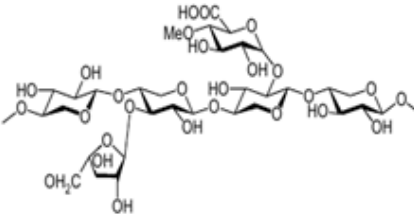
2.5.5.3. Cellulose-Based (Organic) Adsorbents

These are generally derived from biomass especially agricultural wastes with high content cellulose. Biomass contributes up to 14 % of the world's energy consumption meaning its proper use can limit dependency on fossils. Biomass molecules are broken down to release energy in form of heat and biofuels. Biomass is one of the most abundant resources in nature and mainly encompasses cellulose (40-50), hemicellulose (20-40), lignin (20-35), and other extractives which include ashes that make up less than 5 % of the biomass. The composition of woody biomass is given in Table 4

Cellulose ($C_6H_{10}O_5$) is the most abundant polymer in nature, and it is chemically modified to form its derivatives that are applied in several industrial sectors mainly to
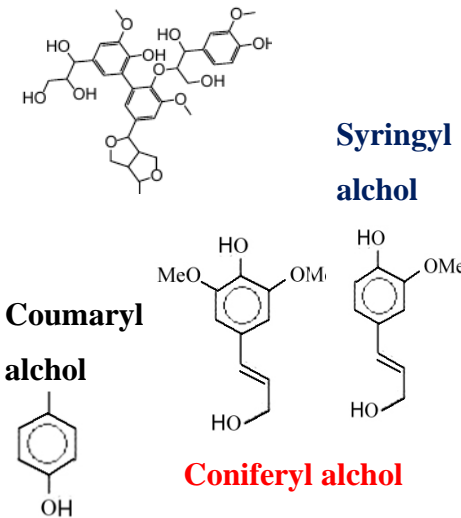
paper, transportation, pharmaceuticals, glass, and ceramics industries. However, the main challenge faced in cellulose application is its poor solubility rate in organic solvents and water. Cellulose is composed of varying proportions of crystalline and amorphous structures based on the source, environment, and origin of the trees. Cellulose physical and chemical properties are affected by the fiber axis and arrangement of the cellulose molecules e.g., amorphous cellulose regions are less orderly and selective to the regents that penetrate through them, so reactions usually take place on the surface of crystallites (Ciolacu, Ciolacu, and Popa 2011; Devabaktuni Lavanya, P.K.Kulkarni, Mudit Dixit, Prudhvi Kanth Raavi 2015)

Table 4. Compositions of Woody Biomass

Name	Structure	Chemical and Physical Properties
Cellulose (D-glucose units) (35–45%)		It's a linear homopolymer linked by glycosidic β $(1 \rightarrow 4)$
Hemi-cellulose (20–30%)		A cross-linked polymer of pentose and hexose sugars. Have an amorphous structure easily hydrolyzed by dilute acids and bases
Lignin (second most abundant polymer)		It's a highly cross-linked polymer and has numerous functional groups. It binds micro fiber cells together giving mechanical strength to plant stems.

Table 4 (cont.)

		Made of hydroxyl and methoxy groups connected by ether bonds. Not hydrolyzed by acids, soluble in alkalis, and hydrophobic.
Others (ashes<5%)	NA	These contain both organic and inorganic substances that are both highly soluble in organic solvents. They also give scent and taste to plants.

2.5.5.3.1. Modification of Cellulose-Based Adsorbents

Adsorbents are modified to increase their selectivity to specific metals from water sources. This can be achieved through mechanical process, thermal process to increase the number of pores in the adsorbent, or chemical process to increase surface area.

Acid treatment is an oxidation process that induces a positive charge on the surface and then enhances the adsorption of positively charged metal ions from aqueous solutions. In adsorbents treated chemically, their structure i.e., chemical bonding between adsorbate molecules and the surface properties of the precursor are altered hence the enhance in adsorption capacity. Chemical modifying chemical agents are acid, basic, or even neutral (Vieira et al. 2014; Abegunde et al. 2020). Some of the adsorption studies directly related to modified adsorbents in literature by the chemical process are summarized in Table 5

Sulfonation: Xu et al. 2020 studied the adsorption of lithium from an aqueous solution onto cellulose after its modification i.e., sulfonation and protonation by grafting glycidyl methacrylate onto cellulose microspheres (CMS) using sulfonation and protonation techniques as shown in Figure 7. The adsorbent exhibited a high lithium adsorption capacity of 16.0 mg/g with Langmuir isotherm. The adsorbent performed well in PH 4-10 range and adsorption-desorption studies showed that the adsorbent can.be reused up to five times (Xu et al. 2020).

Table 5. Comparison of other Organic Lithium Selective Adsorbents

Adsorbent	Experimental conditions (optimum)	Li source	Capacity (mg/g)	Reference
Microcrystalline cellulose (MCC)	Initial concentration of 10mg/L LiCl and adsorption studied at Temp 25,35, 45 & 55 °C	LiCl solution	The optimum adsorbent dosage was 12g ads/L and maximum lithium uptake capacity was 9.60 mg/g at 25 °C	Yaşar Kemal Recepoğlu and Yüksel 2021
Modified activated carbon with multiple MnO_2 nanocomposites ratios	Initial concentration of 20mg/L at PH 12. AC chemically modified with Mn^{2+} solution (0.2,0.15,0.12, and 0.1 M)	Aqueous Li^+ solution (30 mg/L)	(CAC-Mn0.2)-88.5 mg/g, (CAC-Mn0.15)-69.93 mg/g, (CAC-Mn0.12)-65.04mg/g and CAC-Mn0.1)-50.1 mg/g	Kamran et al., 2019

Table 5 (cont.)

MnO$_2$-decorated biochar composites of coconut shell (CSBC) and rice husk (RHBC)	PH of 12, adsorbent dose of 0.1 g/L, contact time 15 h initial Li$^+$ concentration of 40 mg/L.	Li$^+$ solution	RHBC-Mnx composites-62.85 mg g^{-1} and CSBC-Max - 57.8 mg g^{-1}	Kamran and Park 2020
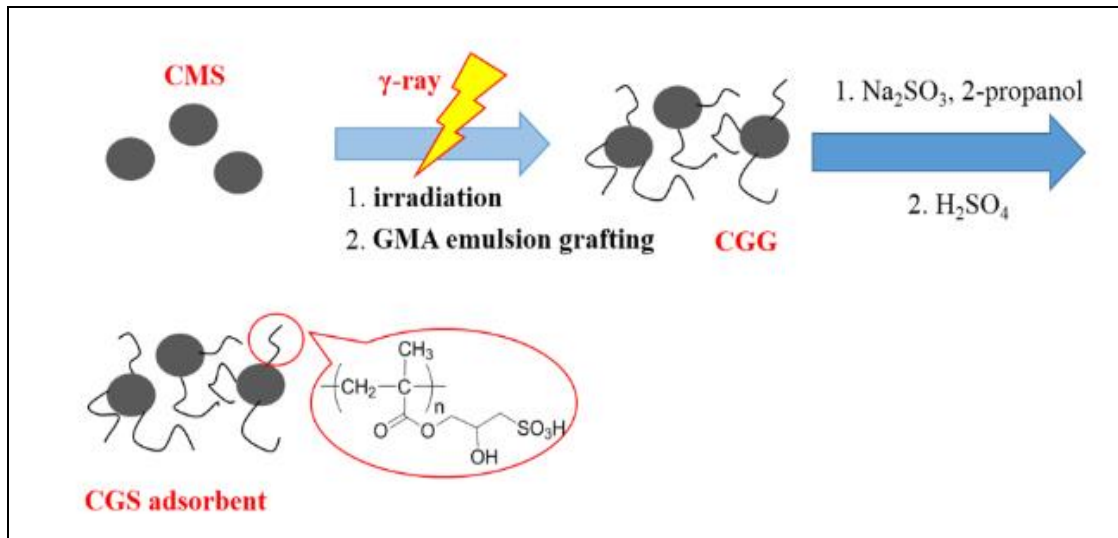
Figure 7. Shows step-by-step functionalization of cellulose by sulphuration

(Source: C. Xu et al. 2020)

Phosphorylation: It changes the structure and characteristics of adsorbents due to attachment of a phosphoryl functional group using phosphorus-containing compounds (phosphoric or phosphonic acid, phosphorus oxyacid's, phosphorus pentoxide, amido phosphates, alkyl, or aryl derivatives of phosphorous acid (Roosevelt, 2015). Modified adsorbents have got several applications especially in textile industries and wastewater treatment, i.e., extraction of metals from water. Phosphorylation is achievable by either shifting esters or ether groups in the cellulose or free hydroxyl groups in positions C2, C3, or C6 (Rol et al., 2019).

Phosphorylation can be performed heterogeneously where phosphoric acid is directly added to cellulose creating a hydrogen atom linked directly to phosphorus as illustrated in Figure 8 or homogeneous phosphorylation where, cellulose is put in contact with molten urea, water, and phosphoric acid and left to interact between 100-

105 °C. In this reaction, phosphoric acid can form ester compounds disubstituted and trisubstituted from cellulose as shown in Figure 9.
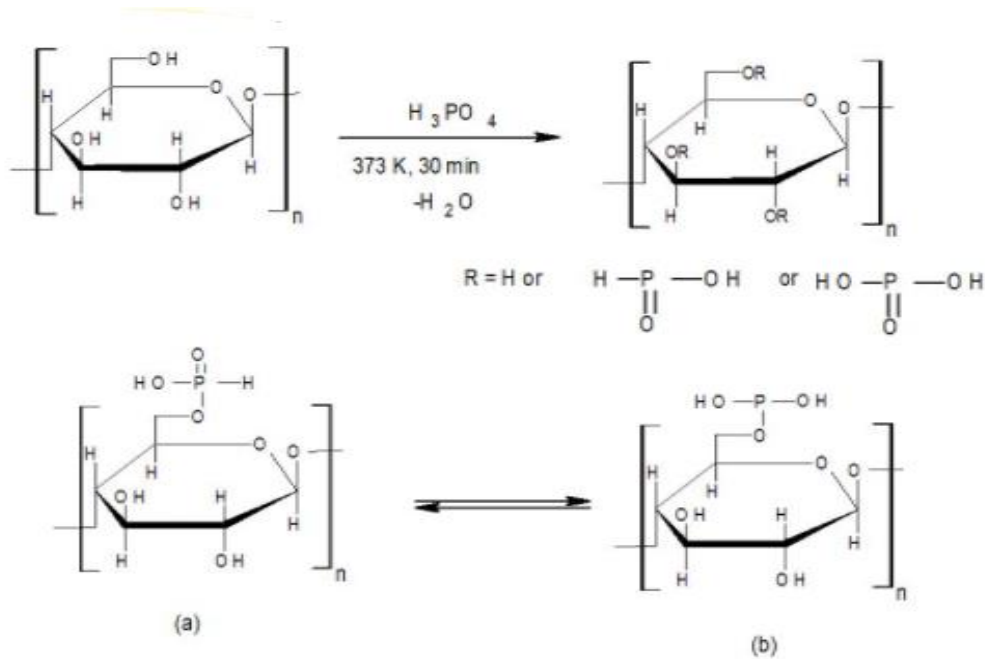
Figure 8. Step by step path of heterogeneous phosphorylation of cellulose
(source: Ghanadpour et al. 2015)
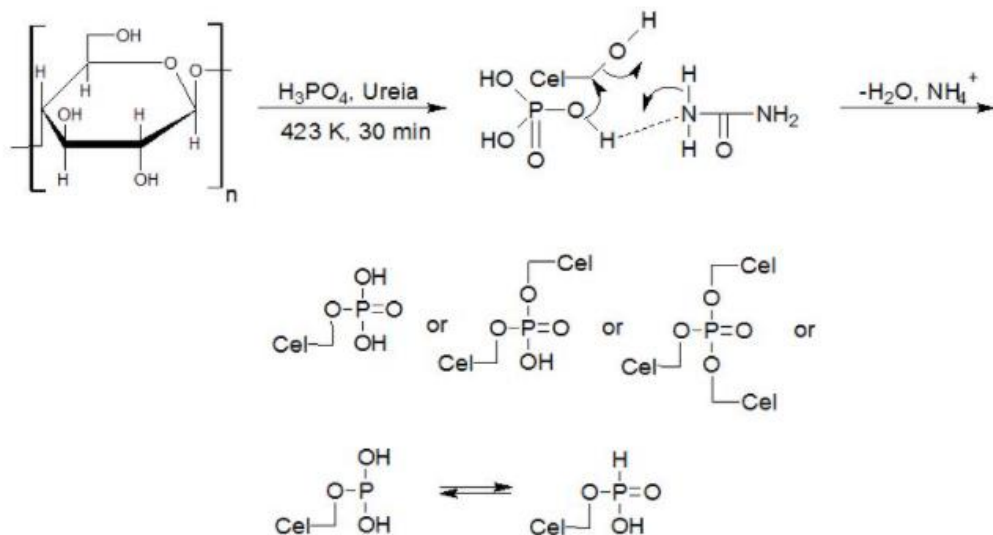
Figure 9. Step by step path of homogeneous phosphorylation of cellulose
(source: Kokol et al. 2015)

Schwantes et al. (2016) studied the adsorption of heavy metals from water using adsorbents synthesized from cassava peels. 7g of adsorbent was chemically modified

with three different solutions 0.1 mol L^{-1} of H_2O_2, H_2SO_4, and NaOH at 60 °C for 6 hours. Langmuir's results proved that adsorption was a monolayer with high adsorption of 19.54 mg Cd (II) per g of $M_{ads.}$ NaOH, 42.46 mg of Pb (II) per g of $M_{ads.}$ NaOH, (45 %) and 43.97 mg of Cr (III) per g of $M_{ads.}$ H_2O_2. (Schwantes et al., 2016)

Activated carbon fiber (ACF) as an adsorbent is mainly favored by its large surface area for adsorption and PAC and GAC classifications are commonly used in wastewater treatment. (Menéndez-Díaz and Martín-Gullón 2006). Also, Liu et al. 2019 extracted methylene blue from an aqueous solution using activated carbon fiber felts with different pore sizes and structures (VACFF-1600 and VACFF-1300). Intraparticle diffusion analysis showed that external and intraparticle diffusions were the rate-controlling steps for the former and only intraparticle diffusion for the latter. Their adsorption fitted well with Langmuir isotherm with an adsorption capacity of 325.83 mg/g and 256.13 mg/g, respectively. (Liu et al., 2019)

Wahid et al (2022) used date pits impregnated with cellulose nanocrystals (CNCs) and ionic liquid (IL) to synthesize lithium adsorbents. Date pits were delignified by using stirring 50g in 6.0 % NaOH for 4 hr. at 70 °C and then bleached with 6.0 % NaClO solution for 2 hr. and 70 °C. Purified cellulose was then treated with 64 % H_2SO_4 for 1 hr. under 25 °C, washed several times then centrifuged for 30 minutes at 5000 pm. Excess sulfate ions were removed by dialysis method for 48 hours, ultrasonicated for 15 minutes at 600 W, and lastly, dried at 70 °C for 24 hours. During adsorption studies, 50 ml of initial Li solutions (5, 10, 15, 20, 25, 30, 35, 50, 70 and 100 mg/L) were added to 0. 05 g of adsorbent. Thermodynamic studies showed it was exothermic and maximum adsorption of lithium of 100 mg/L at PH 6 was obtained (Wahib et al., 2022).

From the literature survey above, it is evident that several lithium extraction methods used at a large scale are greatly limited by the high costs of production, heavy metal disposal as waste, require long durations of time, and lastly, work best with a high initial concentration of metals. On the other hand, the adsorption method performs well at low initial concentration and is environmentally friendly however based on the current literature, all commercial inorganic adsorbents used are still toxic to the environment and ensure a high production cost. This study is to cover this gap using the developed adsorbents beating all the limitations above and also capable of use at a large scale. Concerning organic adsorbents, this is the first study of developing cellulose-based lithium adsorbents from olive branches. Details are given in Chapters 4 and 5.

CHAPTER 3

METHODOLOGY

3.1. Materials and chemicals

The chemicals used in this study were reagent grade chemicals and purchased from Merck.

Chemicals	Chemical formula	Manufacturer
Sodium hydroxide,	NaOH	Merck
Hydrochloric Acid, (37%)	HCl	
Pure Urea	CH_4N_2O	Merck
Ortho-phosphoric acid (85%)	(H_3PO_4)	Merck
Diammonium Hydogyen phosphate.	$(NH4)_2HPO_4$	Merck
Olive branches	NA	NA
Lithium chloride	LiCl	Merck
Sodium chloride	NaCl	Merck
Potassium chloride	KCl	Merck
Magnesium Chloride	$MgCl_2 .6H_2O$	Merck
Sulfuric acid (95-97%	H_2SO_4	Merck

3.2. Adsorbent Synthesis

3.2.1. Collection and Preparation of Biomass

Olive branches were collected from the olive gardens of İzmir Institute of Technology after pruning, thoroughly washed, and dried in the oven at 50 ^oC for 24 hours. The dried biomass was then crushed and sieved in diameters of <250μm, 250-500 μm and >500 μm however, only the 250-500 μm diameter biomass was used in the

experiments since it had a reasonable surface area and much in quantity. <250μm pristine cellulose was used in the characterization of pristine cellulose.

3.2.2. Alkali Treatment Process

40 g of NaOH were thoroughly mixed in 100 ml of water to make 10 M sodium hydroxide in an iced bed on a magnetic stirrer as the reaction was exothermic. 10 g of olive branches were added to the 10 M NaOH solution and stirred thoroughly for 2 hours at ambient temperature. 10 M of hydrochloric acid was added to neutralize the solution and to precipitate out non-cellulosic materials. The mixture was then washed several times with excessive water to remove the chemicals and then filtered. The residue was dried at $70\,^{\circ}C$ for 6 hours and ground to obtain uniform particles.

3.2.3. Preparation of Phosphorylating Chemical Solution

7.8 mL phosphoric acid, 26.4 g diammonium hydrogen phosphate, 60.1 g urea were mixed thoroughly mixed in 150 ml of water. The solution was left to thoroughly mix at 800 rpm at room temperature until it cleared. Urea has been used in numerous studies to prevent the degradation of cellulose, increases cellulose swelling hence increased penetration resulting in high phosphorylation of cellulose.

Phosphorylation: 10 g of alkali-treated olive branches were added to the prepared phosphorylating solution, mixed thoroughly, left to stand at room temperature for 1 hour and, then dried at $105^{\circ}C$ for 18 hours in the oven. The temperature was then increased to $150^{\circ}C$ to allow the reaction to take place for 2 hours. Also, ammonium gas was smelled at this point proving the occurrence of reaction. Phosphorylated olive branches were then washed several times with excess water to remove the suspending chemicals. The residue obtained after filtration was oven-dried at $70^{\circ}C$ for 6 hours. The resulting residue was then ground in the grinder to obtain the functionalized cellulose which was later used in all the experiments. This procedure was carried out several times till enough material for experiments was obtained. (This procedure was adopted from Yabusaki, 2010. Patent No. US 7803937 B).

3.3. Adsorbent Characterization

Characterization was performed on pristine, NaOH treated, and functionalized olive branch branches samples at Integrated Research Centre (TAM) in İzmir Institute of Technology (IZTECH).

Scanning Electron Microscope-SEM (Quanta 250 SEM) was used to keenly determine the morphological structure and surface changes of the synthesized adsorbent. The samples were coated with gold by spraying method and analysis was run at an accelerating voltage range of 3.0-5.0 kV. Samples were all observed under a magnification of 5000X. EDX was used to determine the elemental compositions of all the samples, FTIR-8400S was used to determine the changes in the chemical composition and functional groups in the three samples by analyzing the bond formations and bond breakages. 2 mg of each sample was diluted with 148 mg KBr and pressed into pellets that were then analyzed in the range of 400-4000cm $^{-1}$. BET (Micromeritics Gemini series) was used to determine the surface area, pore size, and pore volume of the adsorbent by using nitrogen as an adsorptive at a saturated pressure of 766.655 mmHg. TGA was used to study the samples' thermal stability by studying the weight change that occurred during the heating of the samples at a constant rate. Lastly, the crystal structure and nature of all the samples was determined by XRD analysis using Siemen's diffractometer D5000 (Berlin, Germany) operating with a generator voltage of 45 Kv, tube current 40 mA, K-Alpha1 with 1.54056 wavelengths, K-alpha 2 with wavelength 1.54439 at a Ratio K-Alpha2/K-Alpha1 0.5, with angle $(\theta-2\theta)$ ranging from 4.99^0 to 80.0^0 with a step size of 0.0167113^0 and counting time 106.045.

3.4. Batch Adsorption Studies

All these studies were performed in a batch mode using 25 ml of LiCl solution and 0.3 g of adsorbent placed in a water bath with a rotation speed of 180rpm until equilibrium. These experiments were repeated twice to minimize the experimental error. Analysis of these samples for determination of Li concentration was done through ICP-OES analysis. Li $^+$ recovery percentage was calculated using Eqn 1 and adsorption capacity was calculated by Eqn 2.

$$R\% = \frac{(Ci-Ce)100}{Co} \qquad\qquad \text{Eqn (1)}$$

$$qe = \frac{(Ci-Ce)V}{M(ads)} \qquad\qquad \text{Eqn (2)}$$

3.4.1. Effect of Adsorbent Dosage on Adsorption

The experiment was carried out to determine the efficacy of the synthesized functionalized olive leaves by using a 10mg/L lithium chloride stock solution at room temperature for 24 hours. The study was carried out with varying adsorbent mass. i.e., 4, 8, 12, 16, 20 g/L each repeated twice in 25 ml of Li solution to reduce the error percentage. Also, the dosage effect was investigated with equivalent adsorbent quantities of Lewatit TP 260 and FOB at 30 ºC.

3.4.2. Initial Concentration-Temperature Effect

25 ml of Li solution with concentrations 10, 25, 50, 75, and 100 mg/L was contacted with 0.3 g of adsorbent at 180 rpm for 24 hours. This study was done with the above varying concentrations at -30ºC, 40ºC, and 50 °C.

3.4.3. pH Effect

The effect of pH on the adsorption of metal ions is one of the most crucial parameters. 25 mL of LiCl solution with varying pH of 2-6 was run in a batch mode using 0.3g of FOB bio sorbent in 50 mL bottles with a shaking rate of 180 rpm. 0.1 M hydrochloric acid and 0.1 M sodium hydroxide solutions were used in the adjustment of the pH levels as desired.

3.4.4. Effect of Competitive Ions on Li$^+$ Recovery

This was carried out in presence of 10 mg/L concentration of each of Li$^+$ from LiCl, Na$^+$ from NaCl, Ca^{2+} from CaCl$_2$, K$^+$ from KCl, and lastly, Mg^{2+} was prepared from Magnesium chloride hexahydrate (MgCl$_2$. 6H$_2$O). 25 mL of the mixture solution was added to a 0.3 g of FOB bio sorbent and left in contact for 24 hours to ensure attainment of equilibrium. The adsorbent was filtered from the solution and the concentrations of the residual ions were determined by ICP-OES. Ca^{2+}, Mg^{2+}, Na$^+$, K$^+$ ions were selected because they exist in actual lithium sources i.e., geothermal water, sea water, and brines (Yuan et al. 2019).

3.4.5. Desorption Studies

Desorption was conducted similarly as sorption except adsorbed Li had to be detached from FOB adsorbent that was saturated with 100 mg/L LiCl. As eluents, NaCl, HCl, and H$_2$SO$_4$ with varying concentrations of 0.25 M, 0.5 M, and 1.0 M of each were used as the eluents of Li$^+$ from the saturated FOB adsorbent - (0.3 g of FOB adsorbent was used in each case), done twice.

3.4.6. Measurement of Li $^+$ and Other Ions' Concentration

Lithium and other ions concentration of samples collected from the experiments was analyzed by ICP OES (Agilent technologies, 5110) and PFP7 Jenway flame photometer.

3.5. Adsorption Isotherm Models

The two common Langmuir and Freundlich isotherm models were employed to study the relationship between lithium ions adsorbed on the synthesized adsorbent. Langmuir isotherm was studied using Eqn 3 while Freundlich was studied using Eqn 4.

$$\frac{Ce}{qe} = \frac{Ce}{qmax} + \frac{1}{qmax\ KL} \qquad \text{Eqn (3)}$$

Where, q_{max} is maximum adsorption capacity in (mg/g), K_L is the Langmuir constant related to the energy of adsorption (L/mg) and qe is the adsorption capacity at equilibrium while Ce is the concentration at equilibrium.

$$\ln(qe) = \ln(KF) + \frac{1}{n}\ln(Ce) \qquad \text{Eqn (4)}$$

In Eqn 2, K_F, and n are the Freundlich constants; If n = 1, n > 1, and n < 1, then the adsorption process is linear, physical, or chemical in its nature, respectively. The shape of the isotherms (R_L) was estimated by Eqn 5

$$RL = \frac{1}{1+KLCo} \qquad \text{Eqn (5)}$$

3.6. Thermodynamics Studies

Standard change Gibbs free energy, entropy, and enthalpy in the adsorption process was calculated with Eqn 6 and Eqn 7 at their respective adsorption temperatures. Where, ΔG^0 is standard change free Gibb's energy (kJ mol^{-1}), ΔH^0 is standard change enthalpy (J mol^{-1}), ΔS^0 is standard change entropy (J mol^{-1}K^{-1}), Ce is equilibrium concentration in solution, qe is the equilibrium Li concentration of the adsorbate and R is the universal gas constant (8.314 J mol^{-1}K^{-1}).

$$\Delta G° = -\Delta H° + T\Delta S° \qquad \text{Eqn (6)}$$

$$ln(ke) = \frac{-\Delta H°}{RT} + \frac{\Delta S°}{R} \qquad \text{Eqn (7)}$$

3.7. Kinetic Studies

Adsorption kinetics is used to explain the adsorption mechanism and adsorption characteristics i.e., the time required for the adsorbate to fully attach to the adsorbent. Li adsorption kinetics experiments were investigated at a rotational speed of 200 rpm in

750 ml of LiCl solution at room temperature. Samples were picked at time intervals; 0, 1, 2, 3 ,6, 9 ,12, 15, 30, 60 and 120 minutes. These were filtered to obtain a filtrate that was analyzed for Li concentration by ICP-OES (Espinosa et al. 2017).

3.8. Presence of Competitive Ions Effect

The presence of other ions other than lithium causes competition of the active sites for adsorption hence, a decrease in lithium adsorption capacity. This study was solution with same concentration of 10mg/L of Na^+, Ca^{2+}, Mg^{2+}, Li^+, and K^+ was prepared. 25 ml of the same solution was added to 0.3 g of adsorbent in 50ml plastic bottles. These were left to interact for 24 hours after which they were filtered, and the resulting solution was analyzed by ICP-OES for the present ion concentrations. the method of analysis was adopted from (H. Xu and Guo 2012).

3.9. Adsorption Column Studies

In this section, the synthesized functionalized olive branches were compared with a lithium selective commercial resin, Lewatit TP 260 using a setup shown in Figure 10. Batch adsorption mode couldn't be preferred due to loss of the bio sorbent during the washing step; hence sorption of lithium was executed through an adsorption column with 12 cm height and 0.7 cm diameter using an initial concentration of 10 mg/L of lithium chloride solution. 1 g of FOB was soaked and then poured into the adsorption column. Sorption took place in a bed height of 1.5 cm at a flow rate of 0.5 ml/min, giving a fraction volume of 3 ml per six (6) minutes (0.5 ml/min). For desorption, lithium saturated FOB was washed several times with water to eliminate unabsorbed lithium in the column from influent solution then desorption of lithium was performed using 5% by weight of sulphuric acid which is approximately 0.51 M H_2SO_4 at a flow rate of 0.12 ml/min collecting 2 ml fraction volume in 16 minutes and 40 seconds. Li^+ concentration in the effluent was measured at premeditated intervals to obtain a breakthrough curve. The same procedure was repeated for Lewatit TP 260 which is a commercial lithium selective resin with properties as shown in Table 6. It must also be noted that based on the current literature, Lewatit TP 260 has not been studied in the adsorption column.

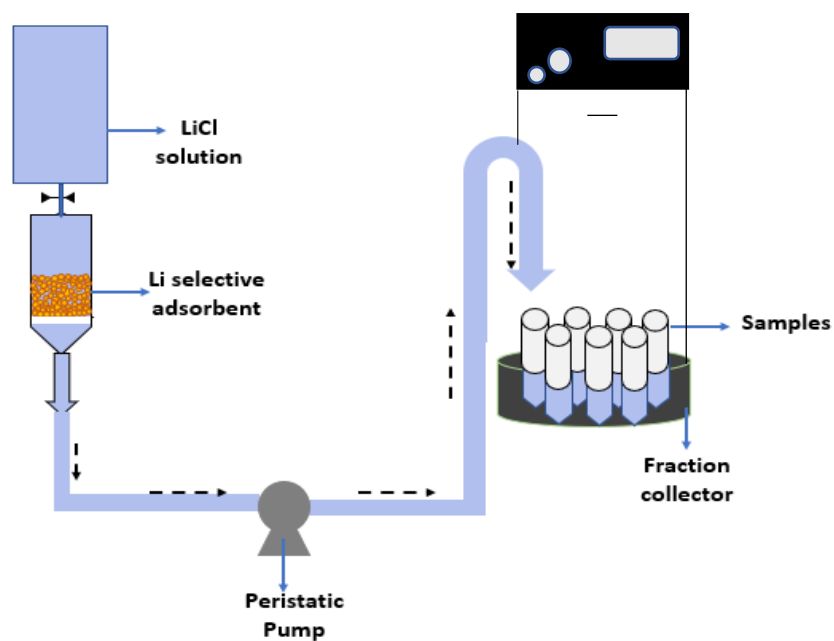**Figure 10.** Schematic experimental set up for column study

Table 6. Lewatit TP 260 Properties

Lewatit TP 260 General Properties	
Ionic form	Ionic form as shipped Na+
Functional group	Aminomethylphosphonic acid
Matrix	Crosslinked polystyrene
Structure	Macroporous
Operating pH-range	1-12

CHAPTER 4

RESULTS AND DISCUSSION

The main objective of this study was to convert olive pruning waste specifically olive branches into an effective lithium selective adsorbent through phosphorylation reaction. Its synthesis is described in Chapter 3 (section 3.2). Characterization of the materials (pristine olive branches (POB), NaOH treated olive branches (NOB), and functionalized olive branches (FOB)), adsorption studies, and factors affecting lithium adsorption, adsorption kinetics, and lastly adsorbent sustainability studies are described in this chapter. The materials are shown in Figure 11 (a), (b), and (c) respectively were characterized by analytical techniques SEM-EDX, FTIR, XRD, TGA, XPS, and BET, also covered in this chapter. There was a significant and observable change in samples' color from light to darker brown as they underwent different chemical modifications.
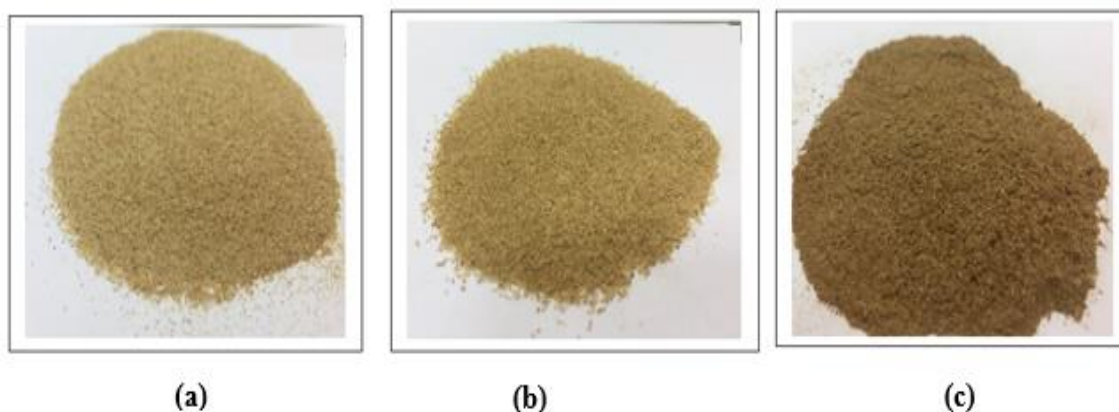
4.1. Characterization Studies

Figure 11. Physical properties of **(a)** POB, **(b)** NOB, and **(c)** FOB

4.1.1. SEM-EDX Analysis

Based on (Figure 12. (a)), POB had a more micro-fibrous structure. In contrast, NOB samples (Figure 13. (b)) had a more porous system (vascular-like formation of

macro fibrils) and the non-uniform distribution of macro fibrils observed can be attributed to the alkali treatment which brokedown the non-cellulosic materials in addition to activation of the hydroxyl groups. These hydroxyl groups on alkali treatment cellulose can adsorbate a detectable amount of adsorbate (Hokkanen, Bhatnagar, and Sillanpää 2016).

Kunusa et al.,(2018) sed the isolation technique for cellulose, alpha-cellulose and microcrystalline cellulose (MCC) from corncobs waste using varying concentrations of NaOH i.e. 4%,6%,8%,10%,12%,14% and 17% solutions and MCC extraction was done using 0.1N HCl. NaOH concentration was proportional to the removal of lignin and hemicellulose. The 8% NaOH yielded the highest crystalline index of 98% and 4% NaOH yielded the highest α-cellulose of 60% with a total yield of 84.5%. SEM results showed the porous /vascular structure and non-uniform distribution of microfibrils in all MCC treated with NaOH 8% and above concentrations. The structure formation was then attributed to fibrillation and damage of fibres to small pieces which increased the surface area of the numerous naked microfibrils (Kunusa et al. 2018). The non-cellulosic material in corncobs-cellulose highly degraded even at lower NaOH concentration unlike NOB because of the higher degree of polymerization in POB than in corncobs-cellulose in addition to the linear chain of β-glucose units joined covalently by 1,4′ glycosidic (C–O–C) links and hydrogen bonds which hold individual strands firmly together forming numerous microfibrils with high tensile strength (Vizárová et al. 2012).

The generated porous and vascular structural formation in NOB samples also increased surface area hence the exposure of binding sites. FOB samples (Fig. 13 (c) at 5000X magnification) became rough and folded which is attributed to phosphorylation reaction of active hydroxy groups in pristine olive brabches and (Fig. 13 (d) at 25000X magnification) displayed FOB with swollen ballons-kind of structure which can be attributed to the effects of urea. Urea prevents cellulose degradation or acts as a catalyst for phosphorylation reaction but is more relatable to the observed swellings in FOB (Figure 12 (b)); it causes swelling of fibers which increases penetration of the reaction reagents (Rol et al. 2020). This may indicate a successful phosphorylation reaction that led to the formation of the active adsorption sites on olive branches cellulose.
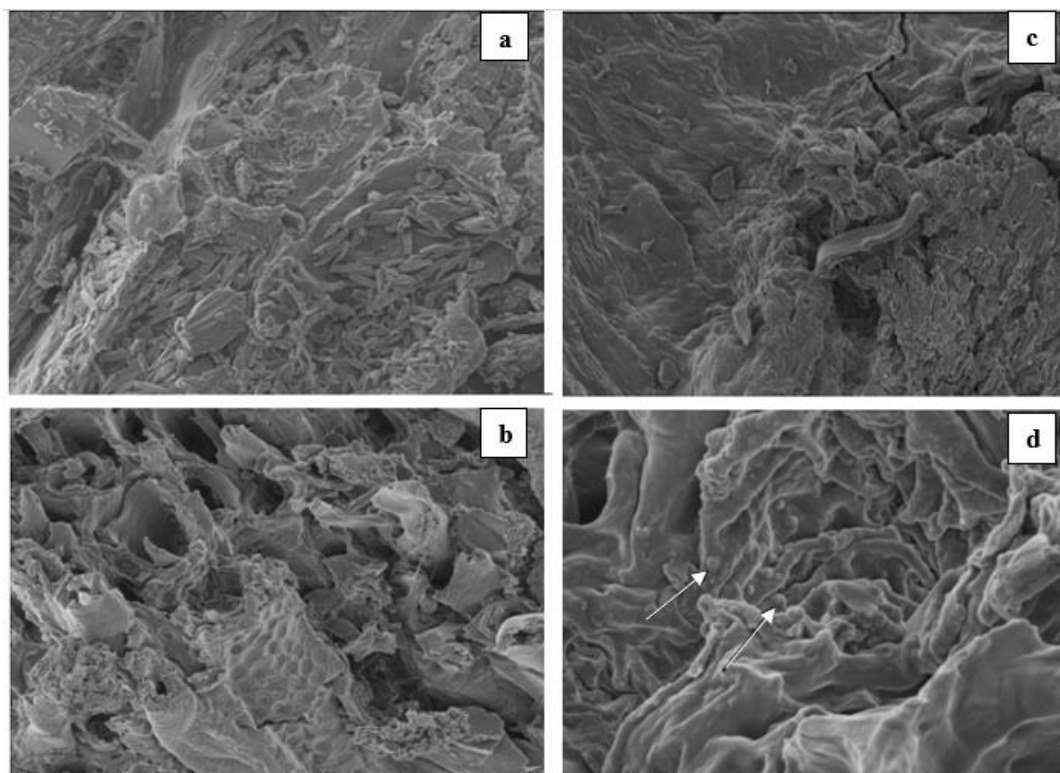
Figure 12. SEM surface morphology images of; **(a)** POB, **(b)** NOB, and **(c)** and **(d)** for FOB at magnification 5000X and 25000X respectively.

Elemental compositions of POB, NOB, and FOB samples in terms of average atomic % are summarised in Table 7 as obtained from EDX analysis (Figure 13) and the mapping results of FOB samples also in Figure 14. The presence of C, N, and O corresponds to actual natural cellulose compositions of biomass however, the quantities of C decreased in NOB, and FOB as a result of degradation of non-cellulosic compounds due to alkali treatment and further modification by phosphorylation respectively but also, some carbonacious material detaches during chemical modifications, suspended and is lost during washing stage of biomass. An increase in O and P was ascribed to sucessful activation of hydroxyl groups and conversion of cellulose to cellulose phosphates i.e. attachment of the phosphorous group onto the structural cellulose of the olive branches. Phosphorous (P) is homogeneously distributed across the FOB material sample as displayed in Figure 14. This high exposure of P also increases the surface area for adsorption. The 6 % increase of N in NOB and FOB was because of exposure of nitrogen covalent bonds in the carbonate moiety e.g., N-C=O and NH_2. Since calcium is not any

part of cellulose structure, it can be concluded that it's an impurity nevertheless it was in diminutive amounts. Table 7 summarizes all the related data in both figures.

Table 7. Elemental composition of POB, NOB, and FOB in average atomic %

	Element Average Atomic (%)				
	Carbon (C)	Oxygen (O)	Calcium (Ca)	Nitrogen (N)	Phosphorus (P)
POB	54.27	38.75	0.64	9.45	0
NOB	52.17	32.17	0.15	15.40	0
FOB	37.59	43.38	0.18	14.65	4.2
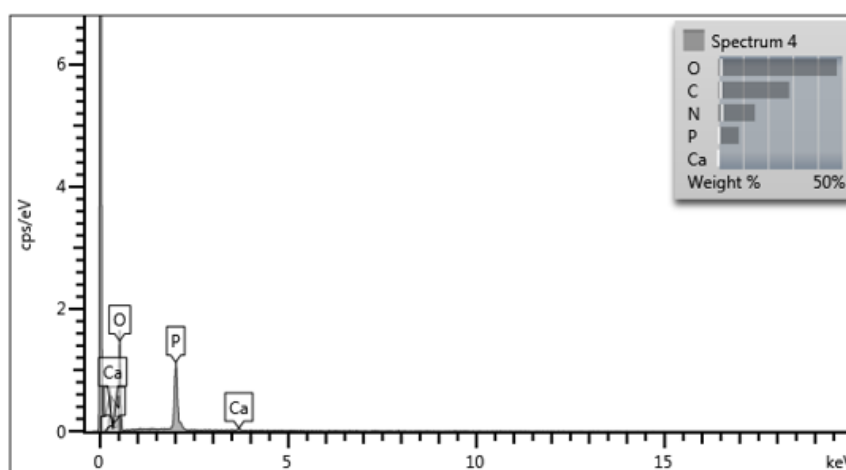
Figure 13. Energy dispersive spectra of FOB
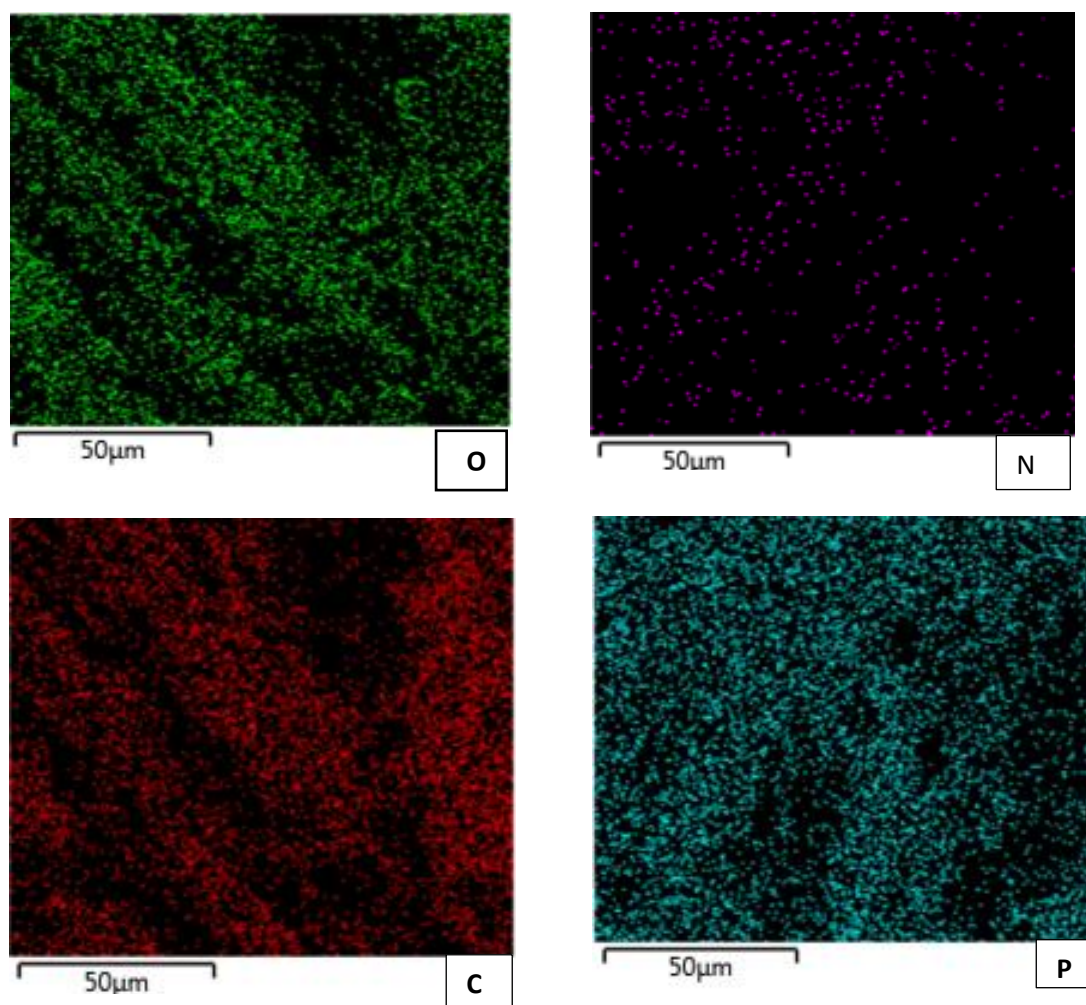
Figure 14. Elemental mappingof FOB

4.1.2. X-Ray Diffraction Analysis (XRD)

XRD was used to study the crystalline and amorphous structure of the three cellulosic samples i.e., POB, NOB, and FOB, and the main diffractions were observed at $2\theta= 43.5°$ (NOB) and $2\theta= 45.1°$ for FOB. The general amorphous nature of the samples POB, NOB, and FOB were attributed to the natural organic compositions of cellulose, hemicellulose, and lignin in all the samples with varying amounts of C, O and N as depicted by the diffractions in Figure 15.

(Figure 15. (a)) POB showed almost no intensive peaks mainly because of the random amorphous structure of lignin that is covalently bonded to hemicellulose which constitutes (20-30)% of biomass (Rahimi Kord Sofla et al. 2016). Alkali treatment removes the most amorphous part of cellulose (lignin and hemicellulose) and this explains the formation of the big peak in NOB, hence the increase in crystallinity index (CrI). Evidential changes of sharper and more visible diffractions were observed (40-48) ° in FOB after phosphorylation (Figure 15 (c)). The (CrI) was calculated using the intensity method and it increased from POB (20.2%), NOB (61.3%), and FOB (72.4%) due to treatments that led to the removal of non-cellulosic components and other residues (Ait Benhamou et al. 2021).
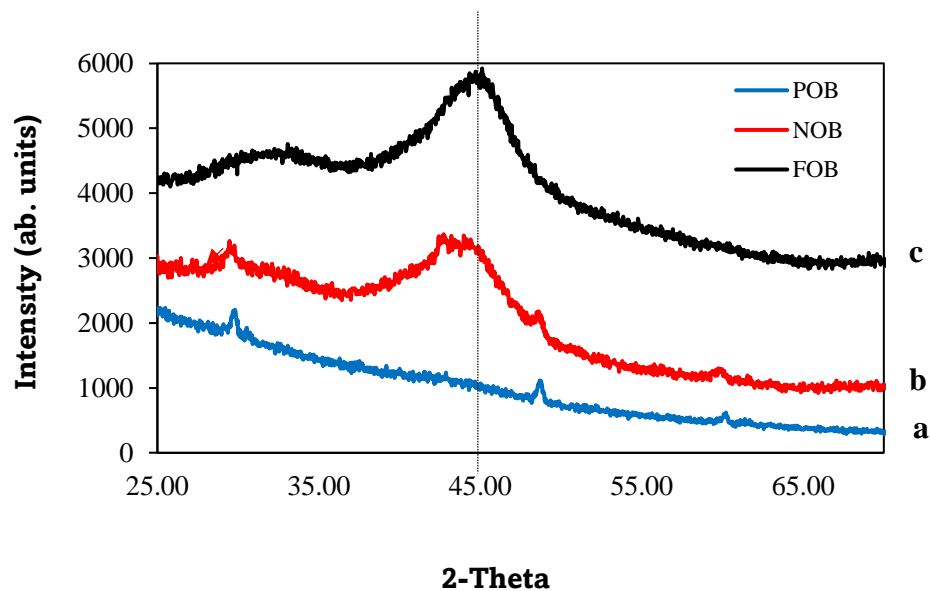
Figure 15. XRD characterization **(a)** POB, **(b)** NOB, and **(c)** FOB.

4.1.3. Fourier Transform Infrared (FTIR) Analysis

The left side of the FTIR spectrums in Figure 16 look similar as it mainly represents the presence of -OH groups (3300-3800 cm^{-1}) and the source of the strong intra-molecular and inter-molecular H-bonding in cellulose (Hishikawa, Togawa, and Kondo 2017; Cichosz and Masek 2020; Rahimi Kord Sofla et al. 2016). The peaks at 2917 and 2847 cm^{-1} in POB are associated with the stretching vibration of C-H formed from CH$_2$ and CH$_2$ groups and these are assigned to lignin components in the biomass

39

(Pacheco et al. 2018; Granja et al. 2001). The same POB peaks were broad, but narrowed and became a bit sharper in NOB. This change is assumed to be due to the activation of the OH groups. Also, this peak is barely visible in the FOB spectrum can be attributed to the phosphorylation reaction which occurred on these primary OH groups of cellulose. (Tzanov, Stamenova, and Cavaco-Paulo 2002). As observed in the POB spectrum, two sharp peaks at 1611 and 1732 cm^{-1} were due to the presence of the carbonyl of an ester group and the carbonyl of a carboxyl group however these two decreased intensities in the NOB spectrum (Abdel-Halim, Alanazi, and Alghamdi 2015; Pacheco et al. 2018; Rahimi Kord Sofla et al. 2016). This change can be attributed to the alkali treatment of POB in which some non-cellulosic composites, e.g., lignin and pectin. The vibration bending 1320 (CH$_2$) wagging at C-6 bending observed in (Figure 16. (a)). POB disappeared in NOB spectrum due to deformation of the CH$_2$-OH bond during an alkali treatment (Granja et al. 2001).

The peak 824 cm^{-1} observed in the FOB sample represents the P-O functional group generated from phosphate groups and supports phosphorylation of cellulose (zhizhin, 1998). The peak at 1648 between (1740-1600) cm^{-1} for -OH resulting from the P-OH group is the weakest and rarely appears on the FTIR spectrums (Hampton and Demoin 2010). The peak 1045 cm^{-1} observed in the FOB spectrum is associated with the stretching and rocking vibrations of the P-O groups of cellulose. The 1137 peak between (1320-1140) cm^{-1} which sometimes ranges to (1415-1085) cm^{-1} due to substituents such as -OH indicated the presence of P=O stretching in FOB and the peak 915 cm^{-1} between (835 -952) cm^{-1} were attributed to the stretching vibration of P–OH bond (Hampton and Demoin 2010; Messa, Faez, and Hsieh 2021; Suflet, Chitanu, and Popa 2006).

Ciolacu, Ciolacu, and Popa (2011) studied chemical structural bonds and composition of amorphous cellulose and observed bonds between (3600-3100) cm^{-1} corresponding to -OH stretching vibrations, C-H stretching bands at 2900 cm^{-1}, (1500-899) cm^{-1}, 1400 cm^{-1} also known as crystallinity band and presenting asymmetric CH$_2$, 898 cm^{-1} assigned to C-O-C stretching at B-(1-4) glycosidic linkages, also mainly present in amorphous cellulose (Ciolacu, Ciolacu, and Popa 2011). Same bonds have been observed in this study but mainly (824-915) observed in this study which also confirms the amorphous nature of cellulose from olive branches obtained in the XRD analysis.
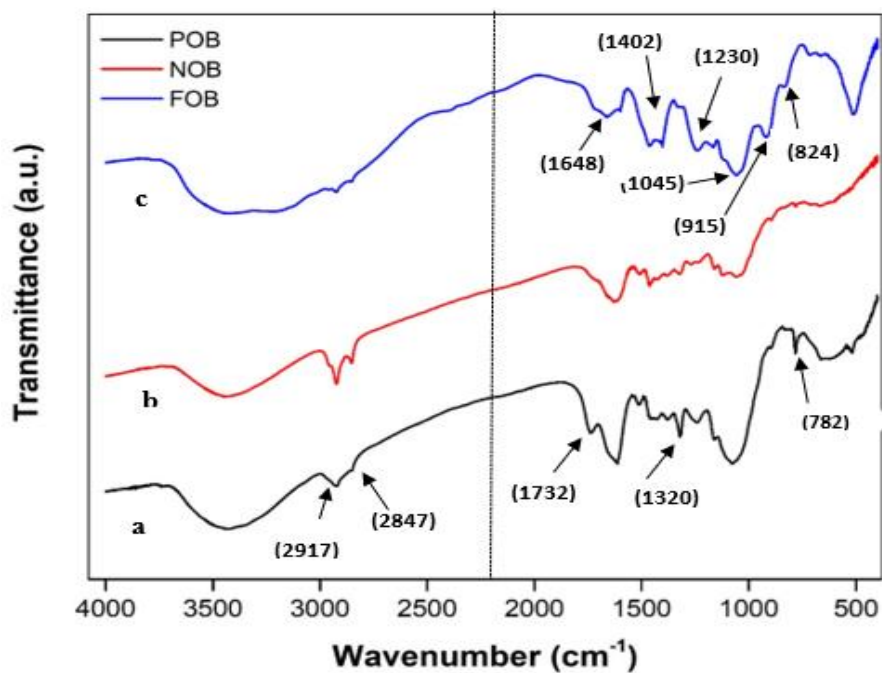
Figure 16. FTIR spectra of **(a)** POB, **(b)** NOB and **(c)** FOB

4.1.4. Thermogravimetric Analysis (TGA)

The TGA graphs in Figure 17 showed four degradation stages of material, i.e., evaporation of adsorbed moisture, cellulose and hemicellulose material decomposition, and carbonization of the materials. The first peaks in Figures 17 (a) and (b) at 73 ⁰C and 79 ⁰C corresponded to evaporation of any adsorbed moisture in samples, which caused weight loss of 4.6% and 21% weight loss, respectively. The second and third stages observed in range (197-400) at 315 ⁰C peak POB and in the range (161-326) ⁰C peak 253 ⁰C in FOB corresponded to thermal degradation of cellulose and hemicellulose, which caused a weight loss of 35.3% and 16.0% in the samples respectively. This significant weight loss is expected since POB contains more cellulosic and non-cellulosic (hemicellulose) materials that degrade through glycosidic bonds decomposition forming volatile compounds. Lastly, peaks at 659 ⁰C in POB and the other at 692 ⁰C in FOB caused a weight loss of 30.1%. This significant loss can be attributed to the carbonization of polymeric material, which occurred between (650-763) ⁰C, requiring a minimum temperature of 500 ⁰C in this study. A similar trend has been reported in similar studies related to the thermal decomposition of phosphorylated cellulose (El-Azazy et al. 2019;

Yaşar Kemal Recepoğlu and Yüksel 2021b). The big weight loss percentage in FOB than NOB is because the phosphorus groups attained during phosphorylation tend to burn at temperatures lower than the onset.
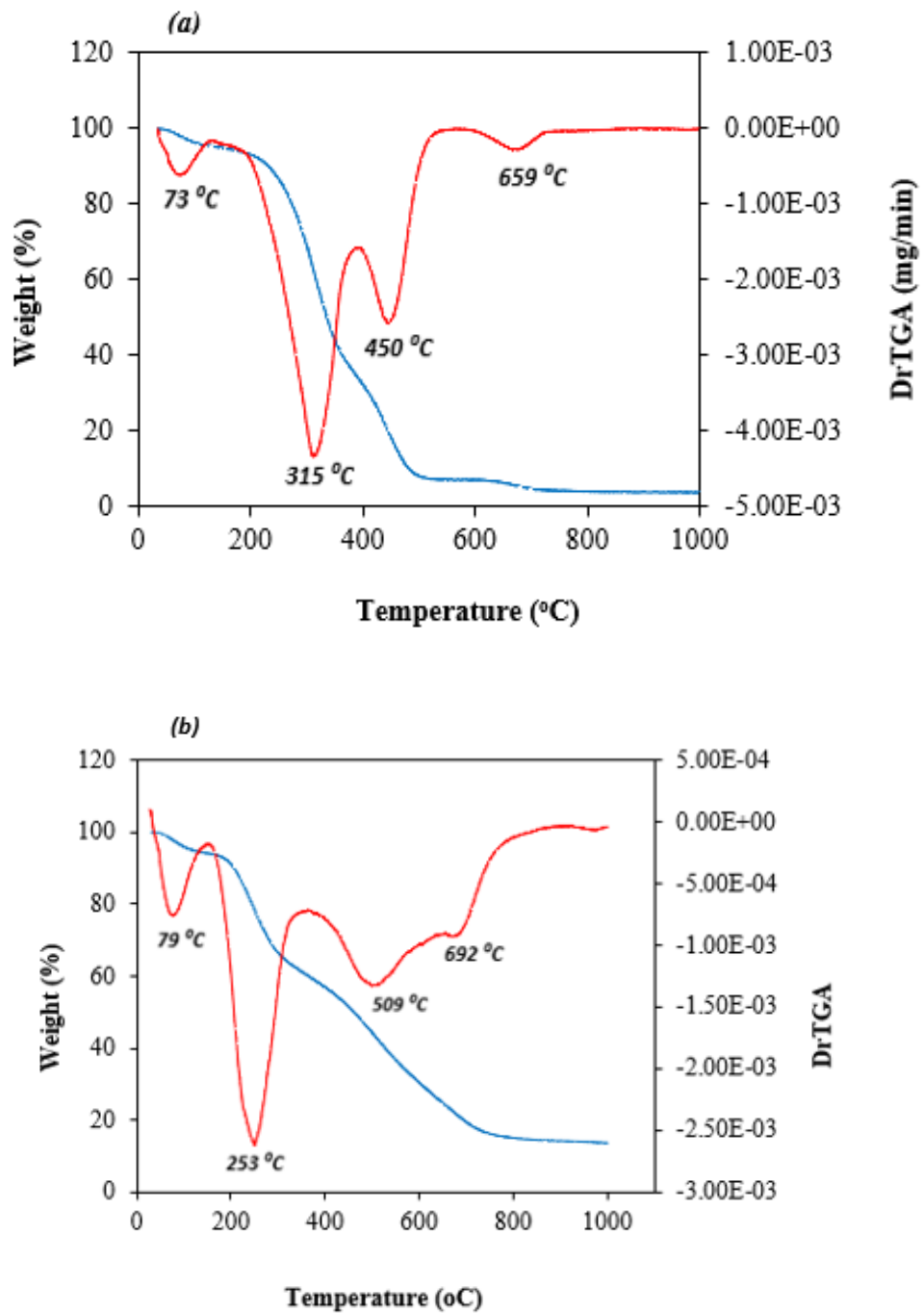

Figure 17. TGA thermal profiles for **(a)** POB and **(b)** FOB samples

Ouazzane et al. (2017) while reviewing the characterization of olive mill solid waste (OMSW) discovered that OMSW thermally decomposed in four stages with the first occurring between (100-200)⁰C, the second and third occurred between (180-500) ⁰C and (250-400) ⁰C and the last one's peak identified to be greater than 500 ⁰C between (100-600) ⁰C. The first phase was associated with moisture loss, the second and third were because of cellulose and hemicellulose degradation in which volatile compounds were produced, and lastly, the high-temperature decomposition above 500 ⁰C was attributed decomposition of lignin and other extractives in the OMSW biomass (Ouazzane et al. 2017). It can be noted that the degradation phases in both studies occurred around the same ranges except for the decomposition of lignin and extractives which took place at temperatures higher than 600⁰C in this study. This drift in degradation temperature may be due to the difference in nature and composition of OMSW (olive pulp, olive stone, or olive solid residues) and olive branches, hence the different quantity compositions (Dermeche et al. 2013).

In studies by Galiwango et al., (2019), it was concluded that the thermal decomposition of cellulose varies temperatures (150-500) °C mainly because of the biomass source hence its composition. Mentha arvensis (250-400) °C, maize straw (300-360) °C, and cotton (230-315) °C (Galiwango et al. 2019).

4.1.5. BET Analysis

Determination of the surface area of the samples is crucial for its enlightenment on the adsorption properties of the adsorbent, and the larger the surface area, the better. BET results further proved the successful removal of lignin and other non-cellulosic material after alkali-treated. Lignin removal is evidenced by the BET surface area increase in the NaOH treated olive branches (NOB) from 1.817 to 2.231 m^2/g, but pore volume and area of POB biomass seem not to have been modified. BET surface area of functionalized olive branches decreased by 71% and this decrease is attributed to the attachment of the functional group in the internal pores of material, the pore volume of FOB also decreased by 75% as a result Detailed BET results of the samples are summarised in Table 8.

In characterization of both chemically modified (by H_2SO_4, HNO_3, and NaOH) and non-modified olive tree prunings (OTP) obtained from Vilches, province of Jaen (Spain), Calero et al. (2013) discovered that BET specific area of unmodified OTP (0.631

m^2/g) decreased with other treatments except for the 1M NaOH treated OTP that increased to 3.526 m^2/g as similarly observed in POB (1.817 m^2/g) and NOB (2.230 m^2/g) in this study. Also, the same OTP obtained the highest number of pores but with the least size (66.38) Å when compared to those treated with H_2SO_4 (107.94) Å, and HNO_3 (91.88) Å (Calero et al. 2013). OTP surface area increased by five times in 1 M NaOH while NOB increased nearly twice in 10 NaOH. One could wonder why the substantial difference in surface areas of OTP and POB yet both were from the same source "olive tree" despite treatment of OTP in low concentration. This may be drawn back to source nature and composition which varies with species diversity and geographical location. Studies have shown the practice of inter-crossing of olive trees and crossing with other plants that caused big olive germplasm after ancestral spreading of olive varieties (Bou Yazbeck et al. 2019).

Table 8. BET surface area and pore size analysis of POB, NOB, and FOB

Material	BET Surface Area (m^2/g)	Pore size-D (Å)	Pore volume (cm^3/g)
POB	1.8166	40.595	0.0010
NOB	2.2299	39.659	0.0012
FOB	0.6446	45.115	0.0003

4.1.6. X-ray Photoelectron Spectroscopy (XPS)

The elemental composition of POB and NOB which showed distinguished peaks attributed to binding energies of C 1s, N 1s and O 1s electrons at signals around 288 (C-C, C-H) 407 and 532 (C=O) Ev in the XPS broad scan spectrums in Figure 18. There was a reduction in C and an increase of O atomic compositions in NOB samples which is attributed to removal of the carbonaceous portions of the biomass. N content peak increased in FOB after phosphorylation which is assigned to nitrogen covalent bonds in the carbamate moiety (NH_2 and N–C=O) at the surface. The formation of new peaks in FOB at signal 134 eV and 190 eV confirmed the presence of P 2p and P 2S electrons respectively, which proved successful phosphorylation in FOB samples most probably at

the surface where the hydroxyl functional groups are easily accessible. This phosphorus is chemically bound to the carbon atoms of cellulose via a C-O-P bonds and this agreed well with micro-FTIR. These bonds originate from phosphate esters which reportedly cause instability of cellulose in aqueous solutions at higher temperatures (Illy et al. 2015; Belosinschi 2021).
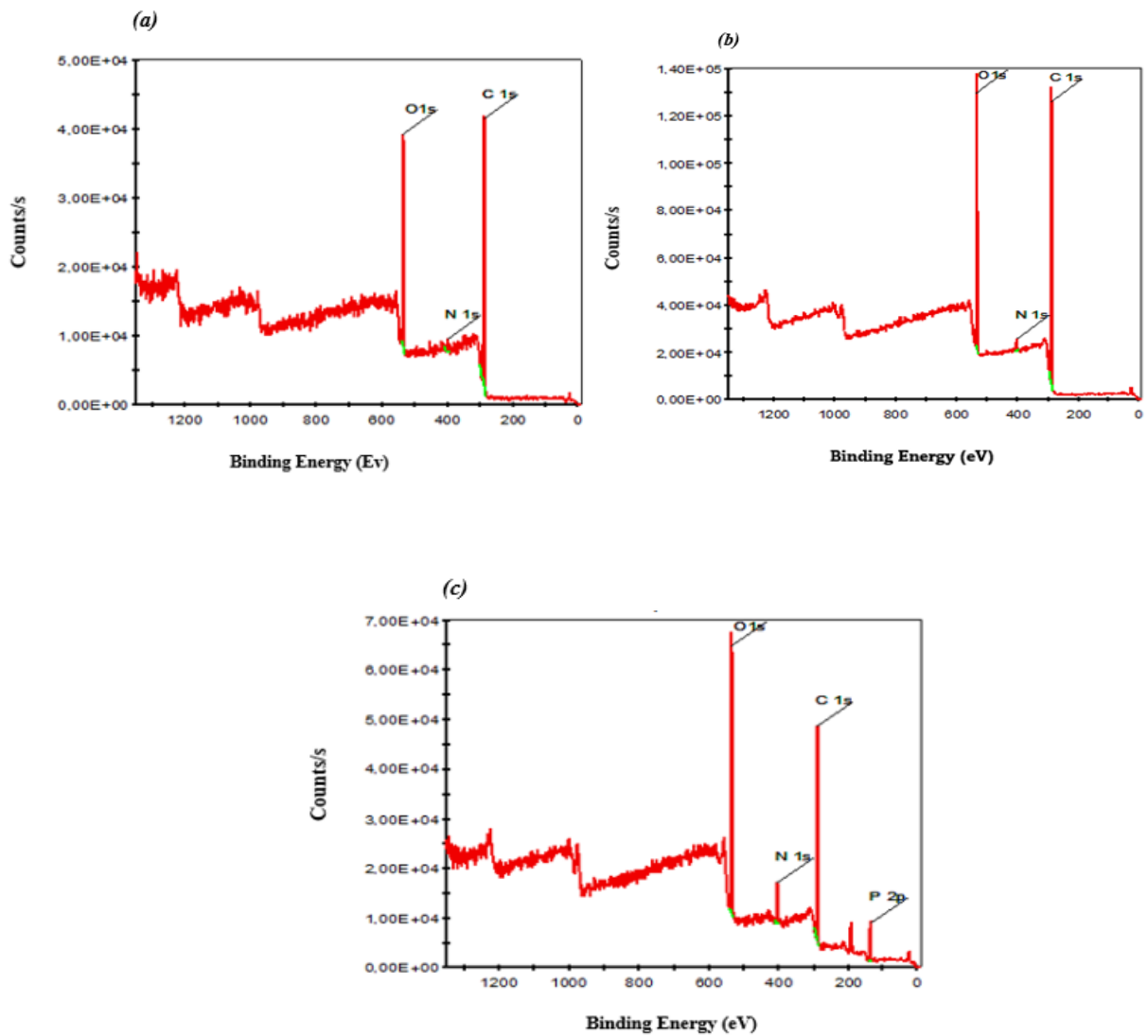

Figure 18. The X-ray photoelectron spectroscopy (XPS) analysis of **(a)** POB, **(b)** NOB and **(c)** FOB.

4.2. Adsorption Studies

4.2.1. Adsorbent Dosage Effect

Li+ removal efficiency gradually increased with adsorbent dosage, i.e., 4 to 20 g/L from 82 % to 88.6 %, until an equilibrium recovery of around 87% at 16 g/L dosages was attained. This dosage was also considered the maximum because a further increase in dosage amount caused no increment in recovery, as seen in Figure 19. Increment of adsorbent dosage led to an increase in the number of available active sites in the solution, hence metal ion recovery. Adsorbent saturation was obtained when dosage increase did not affect metal ion intake due to attained balance in the amount adsorbent active sites to the amount of adsorbate in solution. This trend is not new as similar results have been reported by (Riaz et al. 2009; Quek, Wase, and Forster 1998). At the low adsorbent dosage of 4 g/L, the available amounts of active sites were a bit less than the constant amount of Li ions in 10 mg of Li/L. However, the sites increased with dosage to meet the available lithium ions until almost equilibrium at around 16 g/L. This study used 12 g/L adsorbent dosage as the equilibrium adsorbent dosage in all experiments because its 85 % recovery was good enough as further increment in adsorbent dosage did not have a substantial and reasonable impact, so it is not worth the production costs.
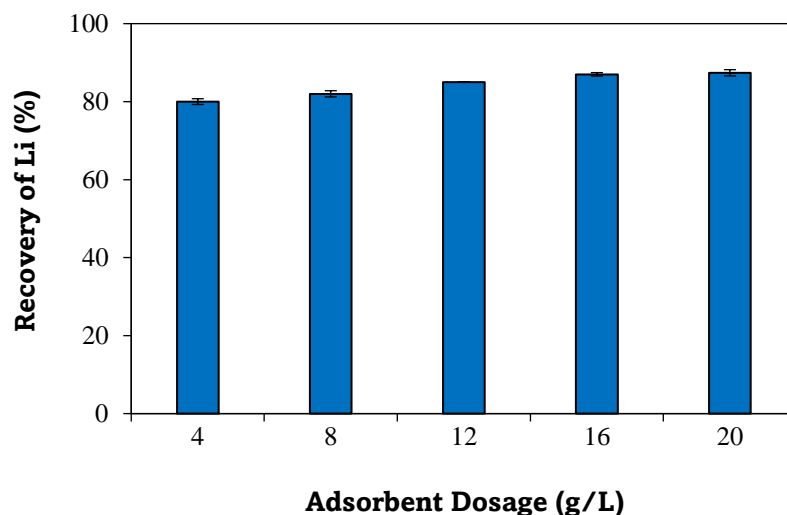

Figure 19. Effect of adsorbent dosage on lithium recovery and adsorption capacity on FOB at 25 ⁰C.

Figure 20. (a) and (b) shows the comparison of Li recovery percentages between the synthesized functionalized olive branches (FOB) and a commercial lithium selective resin TP 260 at 30 ⁰C. Lewatit TP 260 obtained the lowest Li$^+$ recovery of 84 %, while FOB had the least recovery of 76 % at 4 g/L. Equilibrium was observed at a dosage of 16 g/L with 82 % recovery in FOB and 87% in Lewatit TP 260. It is noticeable that adsorbent dosage effect studies in both adsorbents followed the same trend as in Figure 19 despite the different operational temperatures however, FOB performed better at operational temperature, 25 ⁰C than at 30 ⁰C. Li recovery percentages tended to reduce at 30 ⁰C due to the effect of temperature on adsorption as explained in section (4.2.3) of this chapter. Bearing in mind Lewatit TP 260 recovered more Li from solution than FOB because of the reasons explained in section (4.5)
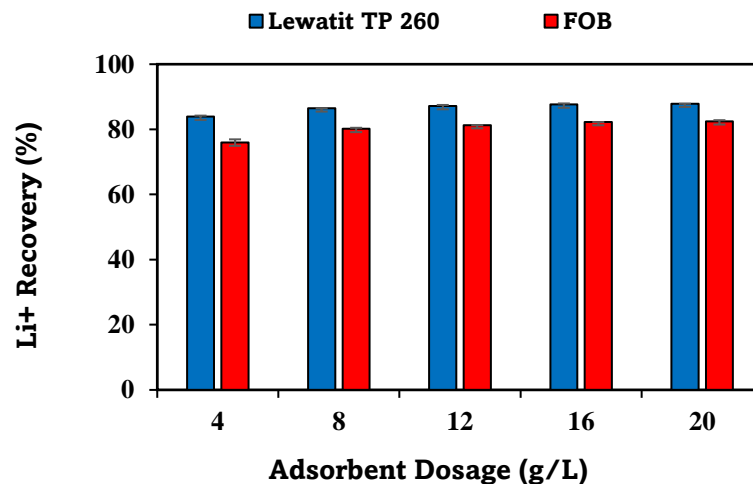
Figure 20. (a) and **(b)**. Effect of adsorbent dosage on Lewatit TP 260 and FOB (Temp =30 ⁰C, Adsorbent dosage 10-20 g/L, Co = 10g/L, speed=180 rpm, pH = (2-8), Time =24 hr)

4.2.2. pH Effect on Lithium Adsorption

The effect of pH on Li$^+$ recovery is given in Figure 21. The highest Li$^+$ recovery of 78% and the lowest 72% were observed at pH 5 and 2. Below pH 2 and 5, it is assumed that the bio sorbent maintained a molecular form and, hence, lower adsorption. In contrast, at pH 5, the functional group on FOB was believed to be ionized, consequently,

increment in sorption of Li$^+$. There was no establish able trend between Li recovery and pH in pH below 6. But it's crucial to note that adsorption experiments were carried out using pH (7.2-8.0) LiCl, 12 g/L adsorbent dosage at 30°C, and the highest lithium recovery of 91.2% was obtained. Therefore, it can be concluded that the adsorption of Li onto FOB is more favourable in slightly alkali pH conditions than in acidic conditions.
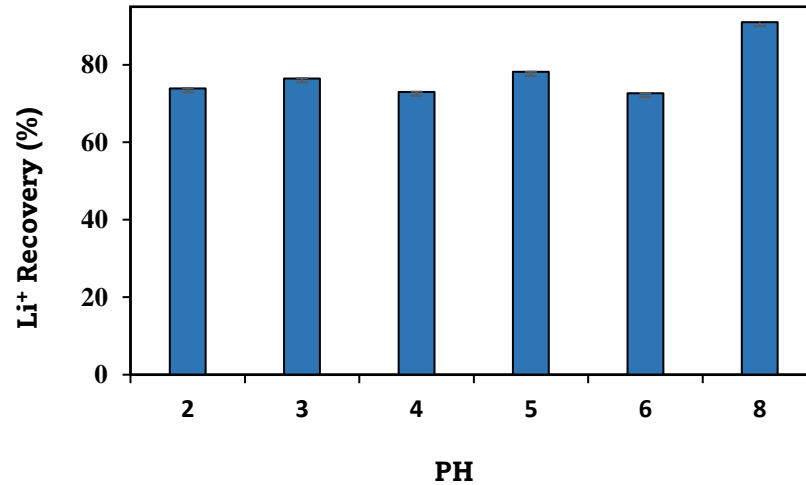

Figure 21. Effect of pH on lithium adsorption onto functionalized olive branches (Temp =30 °C, Adsorbent dosage 12 g/L, Co = 10g/L, speed=180 rpm, pH = (2-8), Time =24 hr)

The zeta potential analysis helped identify the stability of FOB and the charges at the adsorbent surface and solution interface. The effect of Li adsorption on repulsive forces and electrostatic forces was also illustrated. From Figure 22, it can be observed that the point of zero charges (ZPC) value is between 6 and 6.5, an averagely 6.2 value if the initial pH versus change in pH curve is extrapolated to meet the x-axis. A ZPC of 6.2 means that the FOB surface was highly protonated below pH 6.2, which led to competition for active sites between Li ions and the positively charged ions hence the reduction in Li recovery. Similar findings were found in previous studies (Yaşar Kemal Recepoğlu and Yüksel 2021b; Aldawsari et al. 2017).

This same phenomenon explains why a higher recovery rate of up to 91.2% was achieved at pH higher than 6.2, i.e., pH (7.2-8.0); the density of the protons on the FOB surface had reduced hence reduction in competition between the ions. (C. Xu et al. 2020)

deducted that the low lithium recovery in pH< 4 during lithium adsorption onto CGS was due to the surface functional group's H+ and Li+ competition caused by protonation. This also resulted in a positive charge on the adsorbent. Due to Na+ and Li+ competition for active sites on adsorbent in pH 11.2 but a pH >13 destroyed cellulose micropores. This evidence explains why Wahib et al. 2020 found Li highest recovery % of 90% at pH (6-8) and the lowest as 55% at pH 2 when studying pH effect on the recovery of lithium from geothermal water in the pH range (2-10) using date pits impregnated with cellulose nanocrystals and ionic liquid-IL-CNC@DP (Wahib et al. 2022). FOB obtained a higher Li recovery despite its smaller BET specific surface area of 0.6446 m^2/g than IL-CNC@DP with 4.254 m2/g. Therefore, FOB has a higher affinity for Li and is more stable than IL-CNC@DP at pH 6-8.

Ndi Nsami and Ketcha Mbadcam (2013) studied the effect of pH on the adsorption of methylene blue onto activated carbon made from Cola Nut Shells by ZnCl2. The experiment was carried out in an initial pH range (2-8). The highest adsorption of methylene blue was obtained in acidic conditions, i.e., pH 3.5. The surface of the modified activated carbon was fully saturated by negatively charged ions which in turn were equally neutralized by the dense hydrogen ions in solution. However, at PH lower than 3.5, the negatively charged ions on AC were outnumbered by increased hydrogen ions hence an increase in electrostatic repulsion, which led to decreased adsorption. The opposite happened at PH higher than 3.5 until pH 7 when the dye removal rose. This unexpected change was anticipated to come from the demethylation of methylene blue into other dye forms in the literature (Ndi Nsami and Ketcha Mbadcam 2013).

Therefore, it can conclude that the pH of the solution plays a crucial role in adsorption/metal ion recovery and is highly favored at states where the protonation in the model solution is in equilibrium with the charge density on the adsorbent surface. Not to forget the stability /nature of the adsorbate in question.
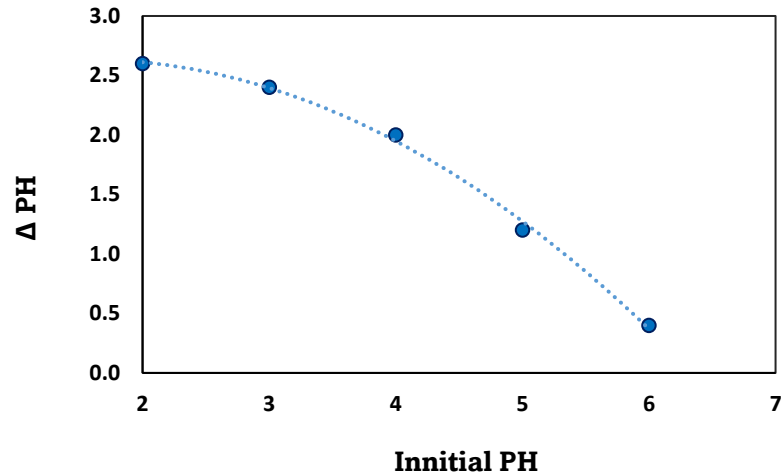
Figure 22. pH initial versus pH final plot for determination of the point of zero charge

4.2.3. Effect of Initial Concentration and Temperature

Two parameters were studied in this section, i.e., temperature and initial ion concentration. Lithium recovery decreased with the increase in LiCl solution's initial concentration and temperature (Figure 23). At the highest Li recovery (91.2 %), it is presumed to have enough/even more active adsorption sites for/than the available adsorbate ions in the solution. However, this ratio becomes un proportional as the adsorbate ions in the solution exceed the available spots on the adsorbent leading to a decrease in adsorption since the adsorbent dosage is constant (Chen and Wang 2008; Farhan and Khadom 2015).

An increase in temperature caused a decrease in lithium recovery; (91.2 - 66.3) % at 30 ℃, (90.6- 65.4) % at 40 ℃, and (88.2-63.1) % at 50 ℃. This decrease in Li^+ recovery indicated that low temperatures favoured its adsorption onto FOB, hence an exothermic reaction. An increase in temperature also weakens the attractive forces between the adsorbent surface and ions in the solution (Tirtom et al. 2012). Despite 30 ℃ acting as the optimum temperature for this reaction in the experiment, it can not be conclusive. If the adsorption reaction is exothermic, then temperature below 30 ℃ is expected to showcase a higher adsorption capacity than 91%, i.e. (91-100)%. Adsorption capacity increased with an increase in initial Li^+ concentration due to the availability of enough

vacant, active sites on the adsorbent and the high Li-ions concentration that enhanced occupancy of the accessible, functional areas of the adsorbent. This is due to the increased Li^+ mass transfer solution onto the adsorbent surface and hence the increase in adsorption capacity. Samra et al. (2014) also attributed it to increased internal diffusion of Li^+ into pores of the adsorbent, which is a driving force for adsorption capacity. This study obtained the highest adsorption capacity of 5.4 mg/g at 30 ⁰C in this study (Figure 24).

Sasha (2010) studied the effect of temperature on adsorption of 300 mg/L concentrated methyl orange (MO) onto chitosan and found out that the adsorbed amount of MO increased (53.33- 95.55) mg/g with an increase in temperature (25-55) ⁰C due to increased diffusion rate of adsorbate from the external boundary layer into the internal pores. It was also reported that the pore sizes of chitosan adsorbent tend to increase with temperature increase hence a minimal intraparticle diffusion resistance causing increased adsorbate intake (Saha 2010).

A higher adsorption capacity was obtained in adsorption MO onto chitosan than Li onto FOB because the former was an endothermic reaction in which temperature enhanced pore formation on chitosan while temperature increase in the latter dismantled the attractive forces responsible for adsorption. In addition, the major difference in adsorption capacity of the above two adsorbents can also best be explained by the difference in their BET-specific surface areas to their particle sizes. Chitosan (≤100 μm) had an average specific area of 4.56 ± 02 m^2/g while POB ($\leq$ 250 μm) only had 1.8166 m²/g. In addition, FOB used in the adsorption experiment had a specific surface area of 0.6446 m²/g for particle sizes roughly between (250-500) μm. Therefore, the more significant specific surface area in chitosan than FOB greatly enhanced its higher adsorption capacity.
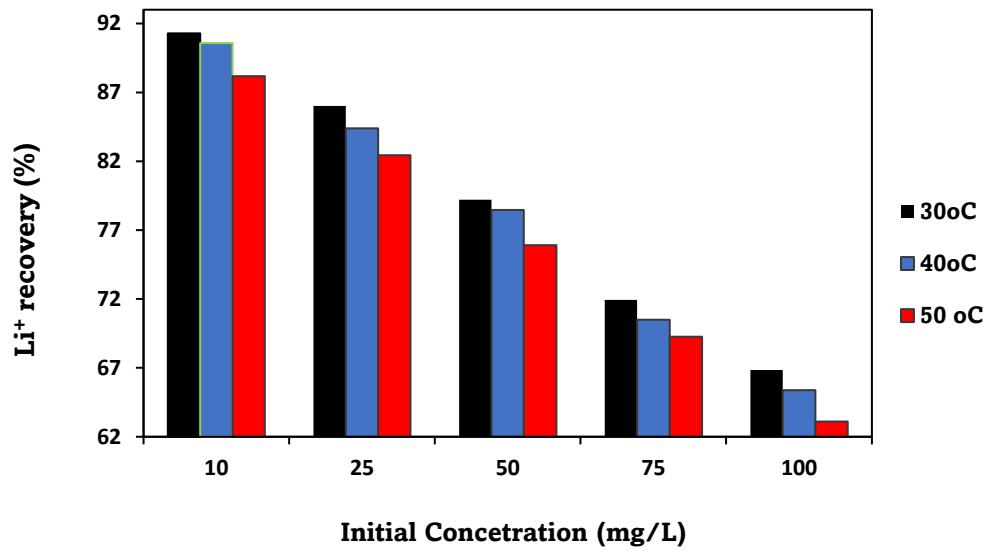
Figure 23. Initial concentration effect on lithium recovery
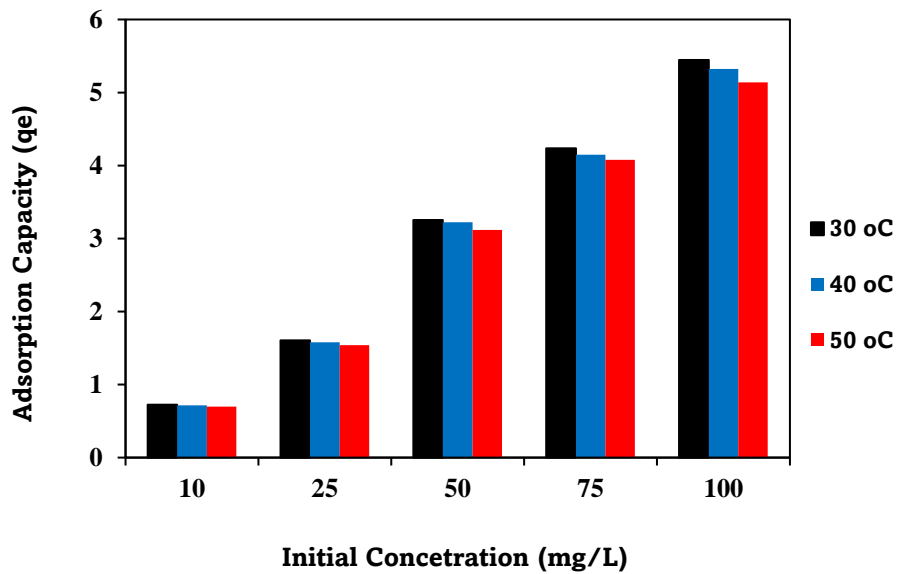(T= 30-50 ⁰C, Co =10 -100 mg/L, adsorbate dosage = 12.0 g/L)

Figure 24. Effect of initial concentration on adsorption capacity.
(T= 30-50 ⁰C, Co =10 -100 mg/L, adsorbate dosage = 12.0 g/L)

4.2.4. Effect of Competitive Ions on Li $^+$ Recovery

The effect of competitive ions on the adsorption of Li in the model solution was studied to determine the efficacy of the other metal ions in actual wastewater and aqueous lithium sources but more importantly the capability of the synthesized potential bio adsorbent (FOB) in presence of metal ions other than Li^+. The adsorption recovery percentage of lithium reduced from 91.2% to 85.3 %. This reduction was caused by the increased competition of Li^+ for unoccupied sites with other ions in solution, and Mg^{2+} had the highest recovery of 98.7%. the metal ions showed an affinity order of $Mg^{2+} > Ca^{2+} > Li^+ > K^+ > Na^+$ with $98.7 > 85.7 > 85.6 > 80.6 > 56.4$ recovery (%) as in Figure 25. The order of affinity for the active sites on the adsorbent is in respect to their ionic sizes which justifies the adsorption rate order. Li^+ exhibited a relatively high competition with the divalent ions, attaining Li recovery % more equivalent to Ca^{2+} ions. This finding indicated a high affinity of FOB to bind with Li^+.

Li et al. (2003) studied the effect of the presence of Pb^{2+}, Cu^{2+} and Cd^{2+} ions on multiwalled carbon nanotubes (CNT) and found out that the adsorption capacity of each ion decreased when other ions were introduced in their respective solutions. Pb^{2+} (97.08 - 34.01) mg/g, Cu^{2+} (28.49- 17.04) mg/g and lastly, Cd^{2+} showed the lowest affinity for active sites (10.86- 3.3) mg/g at pH 5.0. Similarly, Pb^{2+}, Cu^{2+} and Cd^{2+} exhibited affinity in the order of their ionic sizes i.e., $Pb^{2+} > Cu^{2+} > Cd^{2+}$. The adsorption capacity of metal ions decreased with an increase in ionic strength (Y. H. Li et al. 2003).

In conclusion, the metal ions with the biggest ionic diameters highly compete for the active sites than smaller ions in the solution. Also, the presence of other ions in solution is assumed to enhance the collision of ions leading to a general reduction in their mass transfer hence low adsorption.
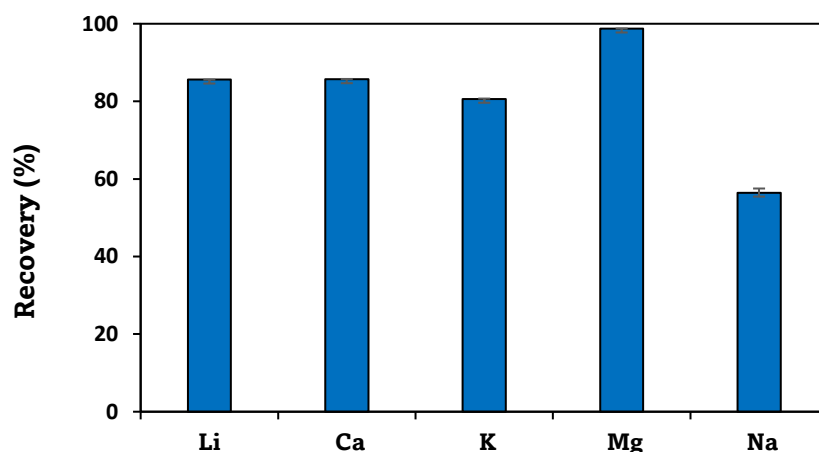
Figure 25. Effect of competitive ions on Li^+ recovery by FOB
(Co =10 mg/L each ion, T =25 °C, adsorbate dosage = 12.0 g/L)

4.2.5. Desorption Studies of Li^+ FOB

Elution of Li^+ adsorbed onto FOB was crucial because it gives a picture of its reusability at an industrial scale. However, the main objective of this experiment was to determine how much of the adsorbed Li onto FOB can be retrieved for its applications discussed in Chapter 2 (section 2.3). FOB bio sorbent saturated with 100 mg/L of Li was used in this study and it exhibited excellent desorption properties as the lowest desorption percentage was 92% in 0.25 M H_2SO_4 eluent, and the highest 99.9% was observed in 1.0 M NaCl eluent. However, all three eluents generally exhibited the excellent desorption capacities with 0.5 M H_2SO_4 at 98 +/- 0.2%, 1.0 M HCl at 99.6 +/- 0.2%, and 1.0 M NaCl at 99.99 +/- 0.2% for all (Figure 26). In conclusion, FOB exhibited a high and excellent desorption efficiency. The regenerated FOB bio adsorbent can be reused for recycling (The number of recycles for FOB could be established using adsorption-desorption isotherms in future research).

In literature, Papaoikonomou et al (2021) conducted the desorption of phenolic compounds from activated and non-activated carbon adsorbents sourced from pomegranate seeds. Three batches were run in 50% acetic acid (pH 1.2), water (pH 7), and alkaline water (pH 12.0) solutions to establish the best desorption conditions. The acidic conditions proved the most efficient solution with the highest desorption efficiency

of 8.1, 45.9 and 73.2, % for non-activated, thermally activated, and chemically activated carbon, respectively hence a chemisorption reaction. Desorption in thermally activated carbon was mainly hindered by the high bond strength between phenolic compounds and adsorbents (Papaoikonomou et al. 2021).
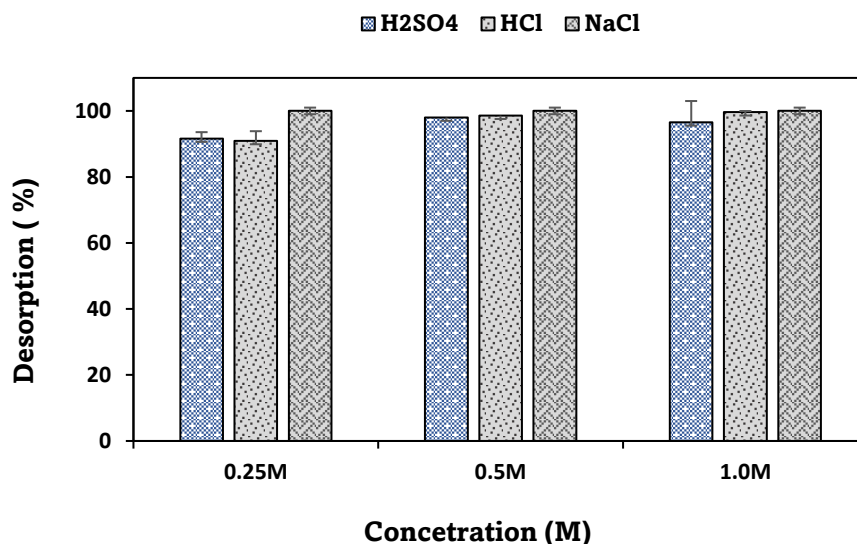
Figure 26. Desorption of Li$^+$ from Phosphorylated Olive Branches (FOB) (Temp =25 ºC, Adsorbent dosage 12 g/L, Co = 100 mg/L saturated FOB, speed=180 rpm, pH = 8, Time =24 hr)

4.3.   Adsorption Performance of Li$^+$ onto FOB Adsorbent

Determination of Li$^+$ performance on FOB was done in both batch adsorption mode and adsorption column setting. Batch mode experimental results were used to determine the adsorption capacities of FOB at temperature 30 ◦C, 40 ◦C, and 50 ◦C.

4.3.1. Adsorption Isotherms

Freundlich and Langmuir's adsorption isotherms were used to describe equilibrium data in this study and determine the better fitting isotherm as this unveils the nature of adsorption. Langmuir isotherm assumes a monolayer formation as adsorption proceeds, and isotherm constants are attributed to the affinity of the binding sites. (Armbruster and Austin 1938). On the other hand, Freundlich isotherm assumes

that the ratios of the adsorbed amount to adsorbent weight per concentration keep varying due to the heterogeneous nature of the adsorbent surface (Kovacova et al. 2020). Standard entropy change (ΔS^o), standard enthalpy change (ΔH^o), and Gibbs free energy were determined using Van't Hoff's equation to better understand the nature of Li ions adsorption onto the synthesized functional olive branches (FOB). The changes of standard entropy change, and enthalpy were calculated from the intercept and slope of the Van't Hoff plot, as seen in Figure 28.

The results show that Langmuir and Freundlich isotherm models were well fitted for adsorption of lithium with a high correlation ($R^2 \geq 0.97$) as seen in Table 9 and Table 10 respectively but still observable that data best suited Freundlich isotherm model (Appendices). Adsorption capacity decreased from 6.7 mg/g to 6.5 mg/g. This decreasing trend in Li adsorption capacity was because molecules gained more kinetic energy as temperature increased, causing a random movement of the ions in LiCl solution hence less interaction with the active sites. The force of attraction between the functional surfaces of the adsorbent and the metal ion decreases with temperature to increased degrees of freedom. This behavior is typical of the biosorption of most metal ions from their solution due to the reaction's exothermic nature and anticipated destruction of bio sorbent structure at higher temperatures (Farhan and Khadom 2015; Sari et al. 2008; Olawale 2020). In addition, Spiff, 2015 also noted that the already attached adsorbates tend to detach from the biomass surface back into a solution, facilitating the trend (Spiff, 2005). The value of nF, which determines the favorability of adsorption, also decreased with temperature increase, which justifies that biosorption is favored more at lower temperatures than higher temperatures (Olawale 2020) as observed in Table 9 below. The decrease in K_L value from 0.1 to 0.08 justified that the binding affinity of FOB to lithium ions in the solution was reduced by the increase in temperature. This result also indicated that surface interactions i.e., hydrogen bonding and Van der Waals interactions influenced Li sorption mechanism more than pore filling in FOB. The high value of n_F i.e., $n_F > 1.0$ or ($0.1 < (1/nF) < 1.0$) in Freundlich isotherm model further justified stronger interaction between FOB and Li ions at temperatures between 30 °C and 50 °C however these interactions also seemed to weaken as temperature increased and this is evidenced by the decrease in adsorption capacity. Similar effect have been observed in adsorption of Cd^{2+} and red food dye (Piccin, Dotto, and Pinto 2011; Vidhyadevi et al. 2014).

Table 9. Langmuir parameters at temperatures 30 ⁰C, 40 ⁰C, and 50 ⁰C

Langmuir Isotherm	30 ⁰C	40 ⁰C	50 ⁰C
Q_{max} (mg/g)	6.7069	6.6269	6.6534
K_L (L/mg)	0.1069	0.0990	0.0827
SSE	0.3824	0.426	0.3161
R^2	0.9752	0.9752	0.9831

Table 10. Freundlich parameters at temperatures 30 ⁰C, 40 ⁰C and 50 ⁰C

Freundlich Isotherm	30 ⁰C	40 ⁰C	50 ⁰C
K_F (L/mg)	0.8252	0.7848	0.6794
n_F	1.8235	1.7969	1.7176
SSE	0.3824	0.426	0.316
R^2	0.9987	0.995	0.995

Table 11. Thermodynamic parameters for adsorption of Li^+

Temperature (K)	$\Delta H°$ (kJ/mol)	$\Delta S°$ (J/mol.K)	$\Delta G°$ (kJ/mol)
303			-24.7825
313	-17.5176	+24.27434	-25.3186
323			-25.2552

The adsorption isotherms (Freundlich) in Figure 27 indicates adsorption capacities decreasing with an increase in temperature in the order of 5.4 >5.3 >5.1 (mg Li/g of adsorbent) at 30 ⁰C < 40 ⁰C <50 ⁰C as initial concentration increased. This isotherm trend indicated multiple layers formation after first layer on FOB during adsoprtion process. Also, low ($\Delta H°$ < 40 KJ/mol) proved Li adsorption onto FOB a physical adsorption aided by the surface interactions i.e., hydrogen bonding and Van-der Waals interactions
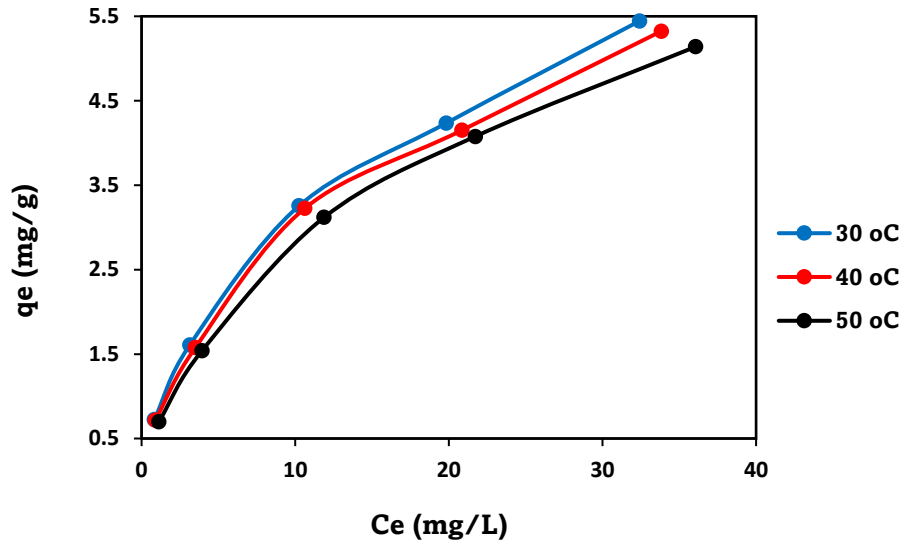
Figure 27. Adsorption isotherms of the phosphorylated olive branches. (Temp = 30-50 ºC, Adsorbent dosage 12 g/L, Co = 10-100 mg/L, speed=180 rpm, Time =24 hr)

Based on Figure 28, it can be deduced the positive trend confirmed an exothermic reaction of functionalized olive branches and the Li-ions during their attachment. The thermodynamic properties of the FOB adsorbent (Table 11) indicate the negative enthalpy proving an exothermic process, positive entropy signified randomness and negative Gibbs free energy signified.
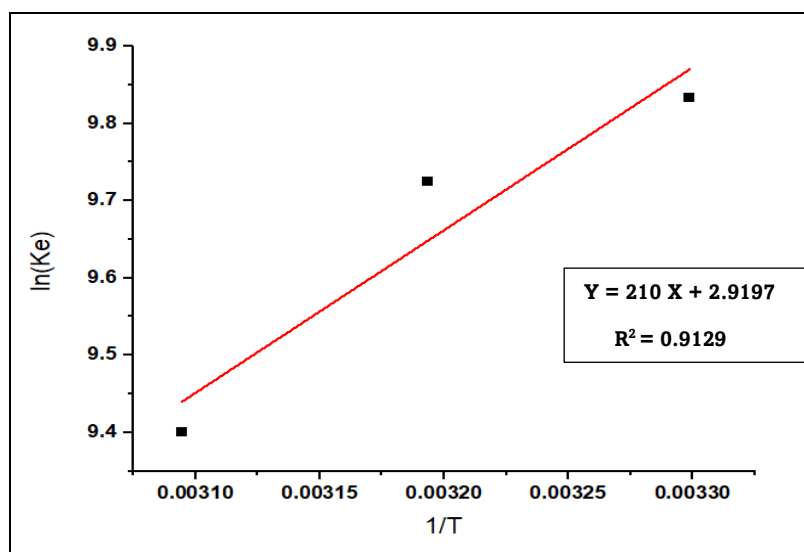

Figure 28. Van't Hoff Equation plot

4.4. Adsorption Kinetics

Contact time was one of the major crucial parameters that influenced the adsorption of Li ions. It demonstrated the recovery of the ions from the solution with repsect to time as in Figure 29. Initially, the Li adsorption rate increased rapidly in the first six minutes for all three concentrations, i.e. 10 mg/L, 50 mg/L, and 100 mg/L. It then reduced gradually until the reaction attained equilibrium at constant room temperature, showing a similar behaviour when lithium adsorbed onto cellulose microspheres with sulfonic acid groups (C. Xu et al. 2020). The fast adsorption in 6 minutes is attributed to the increased concentration gradient between Li ions and FOB adsorbent surface due to the availability of high vacant sites in the first stages. Attainment of equilibrium meant that almost all the active sites had been occupied, causing the remaining Li ions in solution to become asymptotic with the time axis. This phenomenon can be attributed to an increase in repulsive forces due to the presence of the adsorbed ions, making the remaining sites more difficult to access. The presence of these adsorbed ions also slowdown the internal mass transfer within the adsorbent; hence, increment in contact time caused no magnificent change in adsorption. Maximum/equilibrium adsorption capacities of 2.10 mg/g, 3.58 mg/g and 7.10 mg/g were obtained with concentrations 10, 50 and 100 mg/L respectively. Adsorption capacity increased with increased concentration as expected because of the same explanation in section (4.2.3) of Chapter 4.

Gulipalli et al. (2011) discovered that the initial increased rate of adsorption was due to the presence of numerous vacant active sites, which became challenging to occupy with time because of increased forces between ions of adsorbent surface and those still in bulk solution. (Sekhararao Gulipalli, Prasad, and Wasewar 2011). Similar trends have also been observed and explained in other studies (H. Zhang 2014; Riaz et al. 2009; Y. Liu et al. 2003; Benguella and Benaissa 2002).
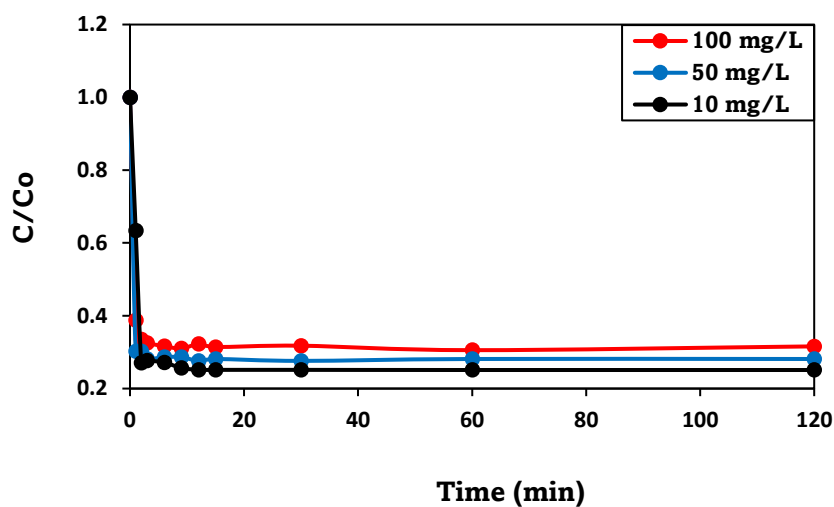
Figure 29. Adsorption kinetics at constant adsorbent dosage (12 g/L) with varying Li$^+$ concentration (Temp =25 ∘C, C_o = (10-100 mg/L, Time = (0-120) min

4.5.   Column Adsorption Studies

An adsorption column experiment was run to simulate the synthesised FOB's practical application and sustainability; 3 ml of aliquots were collected for analysis during adsorption. The saturation of the FOB adsorbent proceeded with elution of lithium using 5 V% H_2SO_4 by collecting 2 ml of aliquots for analysis. The same procedure was performed on Lewatit TP 260. A PFP7 Jenway flame photometer analysed aliquots for FOB and Lewatit TP 260 in Ege university's chemistry department. Calibration before analysis is crucial for adsorption studies, and this was done using 0.1, 0.5, 1.0, 1.5, and 2 mg/L Li concentrations. The curve in Figure 30 was obtained by plotting absorbance vs. concentration through the origin. Based on Beer-Lambert law, the slope 200.84 L.mol^{-1}·cm^{-1} was equivalent to the molar absorption coefficient (ε). Breakthrough curves were constructed by plotting C/Co versus bed volume as shown in Figure 31.

Note: Refer to Table 12 for the complete result summary of Li$^+$ adsorption onto FOB and Lewatit TP 260 in column adsorption mode setup.
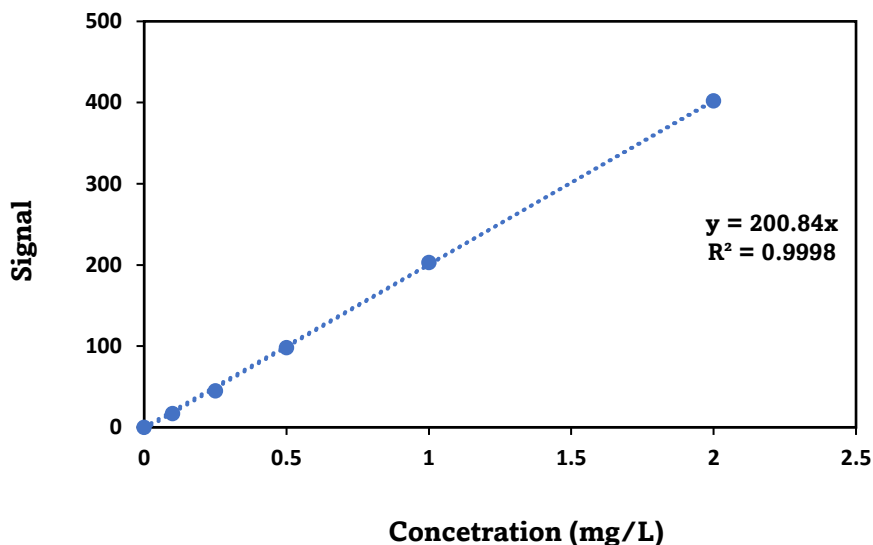
Figure 30. Calibration curve for analysis of Li

The breakthrough curve can be affected by adsorption parameters i.e., initial ion concentration (10 mg/L Li$^+$), flow rate (0.5 ml/min)- and bed height (1.5 cm). However, all these parameters were kept constant as the major objective of column adsorption studies was to study the breakthrough curve of the adsorbents but, more importantly, their capacities and not the variation effect of adsorption parameters in the column. An earlier breakthrough of Lewatit TP 260 at 88 BV indicated a high mass transfer rate at the start that then gradually decreased as adsorption proceeded until almost all sites were occupied, thus saturation of adsorbent. FOB had a slow adsorption rate until breakthrough with a capacity of 2.09 mg Li/ml, but it increased rapidly until saturation as depicted in Figure 31. This higher mass transfer rate in FOB is also evidenced by the steeper breakthrough curve than that of Lewatit TP 260 and more to the left. Lewatit TP 260's breakthrough curve was more to the right which implies that more aqueous Li containing volumes could be treated using Lewatit TP 260 than FOB. Lewatit TP 260 had an overall higher adsorption performance than FOB while FOB exhibited an excellent desorption efficiency of 100% which was twice that of Lewatit TP 260 and degree of column utilization at 57% more than Lewatit TP 260 at 16%. This could be due to FOB's high affinity for Li ions by the phosphoric active sites at the FOB surface that made it easy for Li$^+$ to attach and elute. This high affinity was evidenced in

adsorption kinetics studies. The higher adsorption performance by Lewatit TP 260 could be attributed to the slow adsorption rate after breakthrough which allows more interaction time between Lewatit TP 260 resin and Li ions in solutions or even its functional groups with a high affinity for metal ions. Lewatit TP reached equilibrium at about 850 BV and FOB at around 767 BV, indicating that Lewatit TP 260 could treat a higher volume of solution than FOB (Z. Z. Chowdhury, 2013). Based on the nature of the breakthrough curves in Figure 31, one can easily tell that Lewatit TP 260 performed more effectively than FOB due to the slow absorption rate that allowed the total interaction of Li ions with the adsorbent (Verduzco-Navarro et al. 2020).
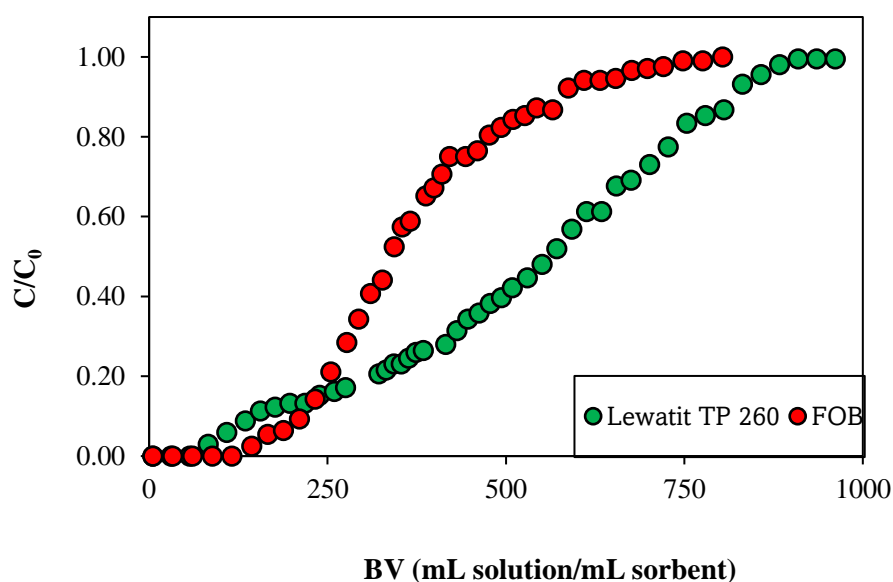

Figure 31. Breakthrough curves of Li^+ sorption on FOB and Lewatit TP 260

Elution trends of FOB and Lewatit TP 260 are illustrated in Figure 32. In FOB, eluent with the highest desorbed lithium concentration was obtained in the region (6-8) BV, and 33 minutes were enough to desorb a maximum of 97% of the adsorbed Lithium from FOB. This performance enhances the FOB adsorbent's application potential. Lewatit TP 260 obtained a more significant elution peak, making sense as it had a higher adsorption capacity. It is worth noting that 99.9 % of the desorption capacity in FOB was achieved in 30 minutes, much higher than Lewatit TP 260 by 47%, in addition to the degree of column utilization more than double that of Lewatit TP 260
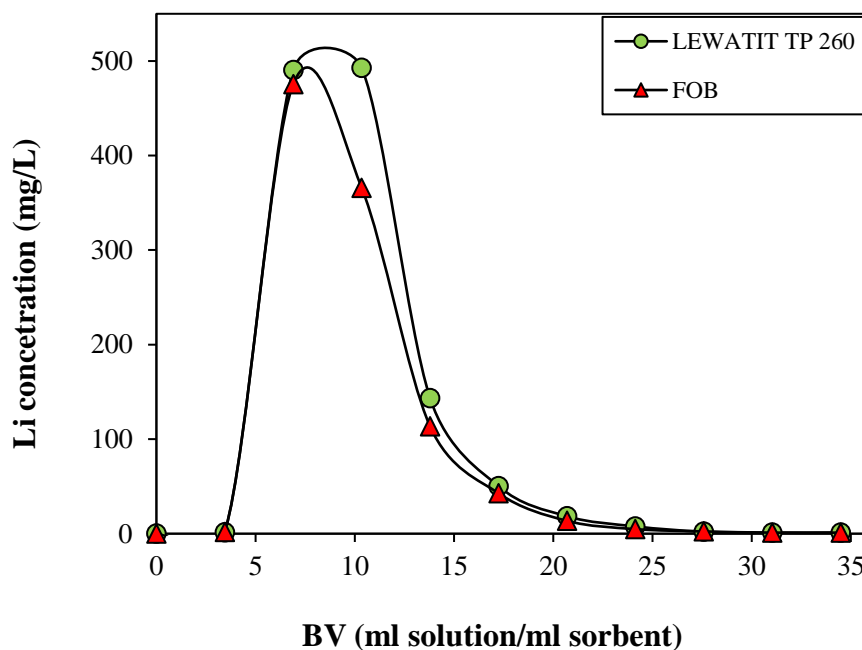
Figure 32. Elution curves of Li$^+$ sorption from FOB and Lewatit TP 260

Table 12. Comparison results summary of FOB and Lewatit TP-260

	FOB	Lewatit TP 260
*Breakthrough capacity (mg Li/ml sorbent)	2.09	1.33
BV for breakthrough capacity (ml solution/ml sorbent)	210	135
Total capacity (mg Li/ml sorbent)	3.67	8.28
BV for total capacity (ml solution/ml sorbent)	734	947
*Degree of column utilization (%)	56.81	16.04
*Desorption efficiency (%)	99.9	50.42

Lastly, based on the assumption of the acceptable effluent concentration of 1 mg/L, Lewatit TP 260 (1.33 mg Li/ml) performed better than FOB (2.09 mg Li/ml sorbent) while FOB exhibited better Li elution and column utilization performance. Considering the main topic of this study; to synthesize an adsorbent capable of recovering

63

lithium from its sources, this lithium must be extracted from its aqueous sources and applied to its deployment areas as discussed in Chapter 2. This puts FOB adsorbent at a higher advantage than Lewatit TP 260.

CHAPTER 5

CONCLUSION

The main aim of this study was to synthesise a lithium selective adsorbent from olive branches waste mainly consisting of olive branches through phosphorylation i.e. grafting phosphoric functional groups.onto FOB. Characterization of NOB samples confirmed successful activation of hydroxy groups and extraction of non-cellulosic materials such as lignin from POB. Moreover, SEM-EDX results for FOB conclusively identified the electron-dense material phosphorous. The homogeneously distributed phosphorous in FOB proved successful attachment and uniform distribution of the phosphorous group, which is also supported in the high adsorption capacity of lithium in the adsorption experiments.

Initial concentration-effect studies showed that Li^+ recovery decreased while adsorption capacity increased with an increase in concentration as expected. A maximum adsorbent dosage of 12 g/L was considered more economical because more increases in dosage increased recovery by only 1 %. Adsorption kinetics studies showed a fast reaction and attained the reaction equilibrium in the first 6 minutes, consequently, the rate determining step of Li adsorption onto FOB could not be determined. Adsorption isotherm parameters characterised Li adsorption by FOB as a physical, exothermic and spontaneous process with high randomness obtaining an equilibrium adsorption capacity of 6.7 mg/g at 30ºC. Experimental data well fitted the Freundlich isotherm model, and n_F >1values (heterogeneity factors) at all temperatures (30-50) ∘C indicated stronger interaction forces between FOB and Li ions on adsorption. Freundlich isotherm indicated multiple layers formation. Also, (ΔH^o <40 KJ/mol) justified Li adsorption onto FOB as physical process aided by the strong interaction forces between Li ions and FOB. The K_L which determines the favorability of adsorption, also decreased with temperature increase (0.1 to 0.08), which justified adsorption was favored by lower temperatures, and Li binding affinity was reduced

Column adsorption studies also showed FOB's potential as a capable adsorbent with a column utilization of 57 %, elution efficiency of 100 % and a breakthrough capacity of 2.1 mg Li/ml sorbent as compared to Lewatit TP 260 with a column

utilization of 16 %, elution efficiency of 50% and a breakthrough capacity of 1.3 mg Li/ml. Lewatit TP 260 exhibited better lithium adsorption properties while FOB exhibited better lithium elution properties and a high.

In addition to batch adsorption studies, column adsorption results showed the fast adsorption and desorption of Li^+, making FOB a potential and efficient Li^+ adsorbent and more probable, a suitable candidate for industrial application.

Based on the experimental result analysis results, the adsorption performance of Li^+ onto FOB is primarily influenced by its initial concentration, pH, and temperature. Based on the evidence by characterisation analysis and biosorption experimental data in this study, it can be concluded that a potential low-cost, sustainable, and efficient novel adsorbent for lithium recovery was successfully synthesized from olive pruning waste consisting of mainly olive branches.

Furthermore, phosphorylated cellulose such as the synthesized FOB (cellulose phosphates) is not only used for extraction of metal ions from water but also applicable to wastewater treatment, food packaging, 3D printing, flame retardancy, but also to biomedical applications (Ait Benhamou et al. 2021) and plastics as flame retardant fillers (Kokol et al. 2015).

REFERENCES

Abdel-Halim, Essam S., Humaid H. Alanazi, and Abdulaziz A. Alghamdi. 2015. "Extraction and Bleaching of Olive Tree Branch Cellulose." BioResources 10 (4): 7136–50. https://doi.org/10.15376/biores.10.4.7136-7150.

Abegunde, Segun Michael, Kayode Solomon Idowu, Olorunsola Morayo Adejuwon, and Tinuade Adeyemi-Adejolu. 2020. "A Review on the Influence of Chemical Modification on the Performance of Adsorbents." Resources, Environment and Sustainability 1 (August): 100001. https://doi.org/10.1016/j.resenv.2020.100001.

Ait Benhamou, Anass, Zineb Kassab, Mehdi Nadifiyine, Mohamed Hamid Salim, Houssine Sehaqui, Amine Moubarik, and Mounir El Achaby. 2021. "Extraction, Characterization and Chemical Functionalization of Phosphorylated Cellulose Derivatives from Giant Reed Plant." Cellulose 28 (8): 4625–42. https://doi.org/10.1007/s10570-021-03842-6.

Akpomie, Kovo G., and Jeanet Conradie. 2020. "Advances in Application of Cotton-Based Adsorbents for Heavy Metals Trapping, Surface Modifications and Future Perspectives." Ecotoxicology and Environmental Safety 201 (May): 110825. https://doi.org/10.1016/j.ecoenv.2020.110825.

Aldawsari, Abdullah, Moonis Ali Khan, B. H. Hameed, Ayoub Abdullah Alqadami, Masoom Raza Siddiqui, Zeid Abdullah Alothman, and A. Yacine Badjah Hadj Ahmed. 2017. "Mercerized Mesoporous Date Pit Activated Carbon - A Novel Adsorbent to Sequester Potentially Toxic Divalent Heavy Metals from Water." PLoS ONE 12 (9): 1–17. https://doi.org/10.1371/journal.pone.0184493.

Alkherraz, Abdulfattah Mohammed, Aisha Khalifa Ali, and Khaled Muftah Elsherif. 2020. "Removal of Pb (II), Zn (II), Cu (II) and Cd (II) from Aqueous Solutions by Adsorption onto Olive Branches Activated Carbon: Equilibrium and Thermodynamic Studies." Journal of Chemistry International 6 (1): 11–20. https://doi.org/10.5281/zenodo.2579465.

Armbruster, Marion H., and J. B. Austin. 1938. "The Adsorption of Gases on Plane Surfaces of Mica." Journal of the American Chemical Society 60 (2): 467–75. https://doi.org/10.1021/ja01269a066.

Ayraktar, O G U Z B. 2007. "Adsorption of Olive Leaf (Olea Europaea L .) Antioxidants On."

Babel, Sandhya, and Tonni Agustiono Kurniawan. 2003. "Low-Cost Adsorbents for Heavy Metals Uptake from Contaminated Water: A Review." Journal of Hazardous Materials 97 (1–3): 219–43. https://doi.org/10.1016/S0304-3894(02)00263-7.

Battistel, Alberto, Maria Sofia Palagonia, Doriano Brogioli, Fabio La Mantia, and Rafael Trócoli. 2020. "Electrochemical Methods for Lithium Recovery: A Comprehensive and Critical Review." Advanced Materials 32 (23). https://doi.org/10.1002/adma.201905440.

Belosinschi, Dan. 2021. "Phosphorylation of Cellulose in the Presence of Urea . Mechanism of Reaction and Reagent Impact . Phosphorylation of Cellulose in the Presence of Urea . Mechanism of Reaction and Reagent Impact .," 0–17.

Benguella, B., and H. Benaissa. 2002. "Cadmium Removal from Aqueous Solutions by Chitin: Kinetic and Equilibrium Studies." Water Research 36 (10): 2463–74. https://doi.org/10.1016/S0043-1354(01)00459-6.

Bou Yazbeck, Elie, Georges Abi Rizk, Alfredo Battistini, Georges Hassoun, Leila Geagea, Rony El-khoury, and Franco Famiani. 2019. "Morphological and Biochemical Characterization of Ancient Olive Trees in Bshaaleh Lebanon." International Journal of Current Research 11 (3): 2337–45. https://doi.org/10.24941/ijcr.34835.03.2019.

Bukowsky, H., and E. Uhlemann. 1993. "Selective Extraction of Lithium Chloride from Brines." Separation Science and Technology 28 (6): 1357–60. https://doi.org/10.1080/01496399308018042.

Bukowsky, H., E. Uhlemann, and D. Steinborn. 1991. "The Recovery of Pure Lithium Chloride from 'Brines' Containing Higher Contents of Calcium Chloride and Magnesium Chloride." Hydrometallurgy 27 (3): 317–25. https://doi.org/10.1016/0304-386X(91)90056-R.

Calero, Monica, Antonio Pérez, Gabriel Blázquez, Alicia Ronda, and Maria Angeles Martín-Lara. 2013. "Characterization of Chemically Modified Biosorbents from Olive Tree Pruning for the Biosorption of Lead." Ecological Engineering 58: 344–54. https://doi.org/10.1016/j.ecoleng.2013.07.012.

Castillo, S., F. Ansart, C. Laberty-Robert, and J. Portal. 2002. "Advances in the Recovering of Spent Lithium Battery Compounds." Journal of Power Sources 112 (1): 247–54. https://doi.org/10.1016/S0378-7753(02)00361-0.

Chen, Can, and Jianlong Wang. 2008. "Removal of Pb2+, Ag+, Cs+ and Sr2+ from Aqueous Solution by Brewery's Waste Biomass." Journal of Hazardous Materials 151 (1): 65–70. https://doi.org/10.1016/j.jhazmat.2007.05.046.

Cheng, Huaigang, Yueyue He, Jing Zhao, Wenting Cheng, and Fangqin Cheng. 2019. "Pilot Test and Cost-Based Feasibility Study of Solar-Assisted Evaporation for Direct Preparation of High-Purity Magnesium Sulfate Hydrates from Metastable Na+,Mg2+//Cl−,SO42−-H2O Salt-Water System." Hydrometallurgy 189 (August): 105140. https://doi.org/10.1016/j.hydromet.2019.105140.

Chitrakar, Ramesh, Yoji Makita, Kenta Ooi, and Akinari Sonoda. 2014. "Synthesis of Iron-Doped Manganese Oxides with an Ion-Sieve Property: Lithium Adsorption from Bolivian Brine." https://doi.org/10.1021/ie4043642.

Christmann, Patrice, Eric Gloaguen, Jean François Labbé, Jérémie Melleton, and Patrice Piantone. 2015. "Global Lithium Resources and Sustainability Issues." In Lithium Process Chemistry: Resources, Extraction, Batteries, and Recycling, 1–40. Elsevier Inc. https://doi.org/10.1016/B978-0-12-801417-2.00001-3.

Cichosz, Stefan, and Anna Masek. 2020. "IR Study on Cellulose with the Varied Moisture Contents: Insight into the Supramolecular Structure." Materials 13 (20): 1–22. https://doi.org/10.3390/ma13204573.

Ciolacu, Diana, Florin Ciolacu, and Valentini I. Popa. 2011. "Amorphous Cellulose - Structure and Characterization." Cellulose Chemistry and Technology 45 (1–2): 13–21.

Dermeche, S., M. Nadour, C. Larroche, F. Moulti-Mati, and P. Michaud. 2013. "Olive Mill Wastes: Biochemical Characterizations and Valorization Strategies." Process Biochemistry 48 (10): 1532–52. https://doi.org/10.1016/j.procbio.2013.07.010.

Devabaktuni Lavanya, P.K.Kulkarni, Mudit Dixit, Prudhvi Kanth Raavi, L.Naga Vamsi Krishna. 2015. "Sources of Cellulose and Their Applications- A Review INTERNATIONAL JOURNAL OF DRUG FORMULATION AND RESEARCH SOURCES OF CELLULOSE AND THEIR APPLICATIONS –." International Journal of Drug Formulation and Research 2 (January 2011): 19–38.

Ding, Yuanli, Zachary P. Cano, Aiping Yu, Jun Lu, and Zhongwei Chen. 2019. "Automotive Li-Ion Batteries: Current Status and Future Perspectives." Electrochemical Energy Reviews 2 (1): 1–28. https://doi.org/10.1007/s41918-018-0022-z.

El-Azazy, Marwa, Sarra N. Dimassi, Ahmed S. El-Shafie, and Ahmed A. Issa. 2019. "Bio-Waste Aloe Vera Leaves as an Efficient Adsorbent for Titan Yellow from Wastewater: Structuring of a Novel Adsorbent Using Plackett-Burman Factorial Design." Applied Sciences (Switzerland) 9 (22). https://doi.org/10.3390/app9224856.

Espinosa, Eduardo, Rafael Sánchez, Rocío Otero, Juan Domínguez-Robles, and Alejandro Rodríguez. 2017. "A Comparative Study of the Suitability of Different Cereal Straws for Lignocellulose Nanofibers Isolation." International Journal of Biological Macromolecules 103: 990–99. https://doi.org/10.1016/j.ijbiomac.2017.05.156.

Farhan, Salah N., and Anees A. Khadom. 2015. "Biosorption of Heavy Metals from Aqueous Solutions by Saccharomyces Cerevisiae." International Journal of Industrial Chemistry 6 (2): 119–30. https://doi.org/10.1007/s40090-015-0038-8.

Flexer, Victoria, Celso Fernando Baspineiro, and Claudia Inés Galli. 2018. "Lithium Recovery from Brines: A Vital Raw Material for Green Energies with a Potential Environmental Impact in Its Mining and Processing." Science of the Total Environment 639 (December): 1188–1204. https://doi.org/10.1016/j.scitotenv.2018.05.223.

Fraga, Helder, Marco Moriondo, Luisa Leolini, and João A. Santos. 2021. "Mediterranean Olive Orchards under Climate Change: A Review of Future Impacts and Adaptation Strategies." Agronomy 11 (1): 1–15. https://doi.org/10.3390/agronomy11010056.

Galiwango, Emmanuel, Nour S. Abdel Rahman, Ali H. Al-Marzouqi, Mahdi M. Abu-Omar, and Abbas A. Khaleel. 2019. "Isolation and Characterization of Cellulose and α-Cellulose from Date Palm Biomass Waste." Heliyon 5 (12): e02937. https://doi.org/10.1016/j.heliyon.2019.e02937.

Gao, Daolin, Xiaoping Yu, Yafei Guo, Shiqiang Wang, Mingming Liu, Tianlong Deng, Yuwei Chen, and Nelson Belzile. 2015. "Extraction of Lithium from Salt Lake Brine with Triisobutyl Phosphate in Ionic Liquid and Kerosene." Chemical Research in Chinese Universities 31 (4): 621–26. https://doi.org/10.1007/s40242-015-4376-z.

Ghanadpour, Maryam, Federico Carosio, Per Tomas Larsson, and Lars Wågberg. 2015. "Phosphorylated Cellulose Nanofibrils: A Renewable Nanomaterial for the Preparation of Intrinsically Flame-Retardant Materials." Biomacromolecules 16 (10): 3399–3410. https://doi.org/10.1021/acs.biomac.5b01117.

Gmar, Soumaya, and Alexandre Chagnes. 2019. "Recent Advances on Electrodialysis for the Recovery of Lithium from Primary and Secondary Resources." Hydrometallurgy 189 (April): 105124. https://doi.org/10.1016/j.hydromet.2019.105124.

Granja, P. L., L. Pouysgu, M. Ptraud, B. De Jso, C. Baquey, and M. A. Barbosa. 2001. "Cellulose Phosphates as Biomaterials. I. Synthesis and Characterization of Highly Phosphorylated Cellulose Gels." Journal of Applied Polymer Science 82 (13): 3341–53. https://doi.org/10.1002/app.2193.

Hampton, Carissa, and Dustin Demoin. 2010. "Tutorial: Sulfur and Phosphorus." Vibrational Spectroscopy.

Hawash, S, E Abd, El Kader, and G El Diwani. 2010. "Methodology for Selective Adsorption of Lithium Ions onto Polymeric Aluminium (III) Hydroxide." Journal of American ScienceJournal of American Science 66 (1111): 301–9. http://www.americanscience.org.

Hishikawa, Yukako, Eiji Togawa, and Tetsuo Kondo. 2017. "Characterization of Individual Hydrogen Bonds in Crystalline Regenerated Cellulose Using Resolved Polarized FTIR Spectra." ACS Omega 2 (4): 1469–76. https://doi.org/10.1021/acsomega.6b00364.

Hokkanen, Sanna, Amit Bhatnagar, and Mika Sillanpää. 2016. "A Review on Modification Methods to Cellulose-Based Adsorbents to Improve Adsorption Capacity." Water Research. Elsevier Ltd. https://doi.org/10.1016/j.watres.2016.01.008.

Hoshino, Tsuyoshi. 2013. "Development of Technology for Recovering Lithium from Seawater by Electrodialysis Using Ionic Liquid Membrane." Fusion Engineering and Design 88 (11): 2956–59. https://doi.org/10.1016/j.fusengdes.2013.06.009.

Ibrahim, Taleb Hassan, Muhammad Ashraf Sabri, Mustafa Ibrahim Khamis, Yehya Amin Elsayed, Ziad Sara, and Barra Hafez. 2017. "Produced Water Treatment Using Olive Leaves." Desalination and Water Treatment 60 (April 2018): 129–36. https://doi.org/10.5004/dwt.2017.0720.

Illy, Nicolas, Maxence Fache, Raphaël Ménard, Claire Negrell, Sylvain Caillol, and Ghislain David. 2015. "Phosphorylation of Bio-Based Compounds: The State of the Art." Polymer Chemistry 6 (35): 6257–91. https://doi.org/10.1039/c5py00812c.

Ince, Muharrem, and Olcay Kaplan Ince. 2017. "An Overview of Adsorption Technique for Heavy Metal Removal from Water / Wastewater : A Critical Review Su / Atıksuda Ağır Metal Giderimi Için Adsorption Tekniğine Genel Bir Bakış : Önemli Bir İnceleme." International Journal of Pure and Applied Sciences and Technology 3 (2): 10–19.

Jiang, Chenxiao, Yaoming Wang, Qiuyue Wang, Hongyan Feng, and Tongwen Xu. 2014. "Production of Lithium Hydroxide from Lake Brines through Electro-Electrodialysis with Bipolar Membranes (EEDBM)." Industrial and Engineering Chemistry Research 53 (14): 6103–12. https://doi.org/10.1021/ie404334s.

Kamran, Urooj, and Soo Jin Park. 2020. "MnO2-Decorated Biochar Composites of Coconut Shell and Rice Husk: An Efficient Lithium Ions Adsorption-Desorption Performance in Aqueous Media." Chemosphere 260: 127500. https://doi.org/10.1016/j.chemosphere.2020.127500.

Kavanagh, Laurence, Jerome Keohane, Guiomar Garcia Cabellos, Andrew Lloyd, and John Cleary. 2018. "Global Lithium Sources-Industrial Use and Future in the Electric Vehicle Industry: A Review." Resources 7 (3). https://doi.org/10.3390/resources7030057.

Khader, Eman Hashim, Thamer Jassim Mohammed, Nourollah Mirghaffari, Ali Dawood Salman, Tatjána Juzsakova, and Thamer Adnan Abdullah. 2021. "Removal of Organic Pollutants from Produced Water by Batch Adsorption Treatment." Clean Technologies and Environmental Policy, no. 0123456789. https://doi.org/10.1007/s10098-021-02159-z.

Kitajou, Ayuko, Takuya Suzuki, Syouhei Nishihama, and Kazuharu Yoshizuka. 2003. "Selective Recovery of Lithium from Seawater Using a Novel MnO2 Type Adsorbent II-Enhancement of Lithium Ion Selectivity of the Adsorbent Low-Temperature Extraction Protocols with Dimethyl Ether (DME) View Project Adsorpsiyon-Elektrodiyaliz Hibrit Prosesiyle Jeotermal Sulardan Lityum Ve Bor Kazanılması (Recovery of Boron and Lithium from Geothermal Waters by Adsorption-Electrodialysis Hybrid Process) TUBITAK-JSPS (Project No. 214M360) View Project." www.ars_separatoria.chem.

Kokol, Vanja, Mojca Božič, Robert Vogrinčič, and Aji P. Mathew. 2015. "Characterisation and Properties of Homo- and Heterogenously Phosphorylated Nanocellulose." Carbohydrate Polymers 125: 301–13. https://doi.org/10.1016/j.carbpol.2015.02.056.

Kovacova, Zdenka, Stefan Demcak, Magdalena Balintova, Cocencepcion Pla, and Inga Zinicovscaia. 2020. "Influence of Wooden Sawdust Treatments on Cu(II) and Zn(II) Removal from Water." Materials 13 (16). https://doi.org/10.3390/MA13163575.

Kunusa, Wiwin Rewini, Ishak Isa, Lukman A.R. Laliyo, and Hendrik Iyabu. 2018. "FTIR, XRD and SEM Analysis of Microcrystalline Cellulose (MCC) Fibers from Corncorbs in Alkaline Treatment." Journal of Physics: Conference Series 1028 (1). https://doi.org/10.1088/1742-6596/1028/1/012199.

Li, Ling, Vishwanath G. Deshmane, M. Parans Paranthaman, Ramesh Bhave, Bruce A. Moyer, and Stephen Harrison. 2018. "Lithium Recovery from Aqueous Resources and Batteries: A Brief Review." Johnson Matthey Technology Review. Johnson Matthey Public Limited Company. https://doi.org/10.1595/205651317X696676.

Li, Yan Hui, Jun Ding, Zhaokun Luan, Zechao Di, Yuefeng Zhu, Cailu Xu, Dehai Wu, and Bingqing Wei. 2003. "Competitive Adsorption of Pb2+, Cu2+ and Cd 2+ Ions from Aqueous Solutions by Multiwalled Carbon Nanotubes." Carbon 41 (14): 2787–92. https://doi.org/10.1016/S0008-6223(03)00392-0.

Liu, Luofeng, Hongwei Zhang, Yushan Zhang, Dongmei Cao, and Xinhua Zhao. 2015. "Lithium Extraction from Seawater by Manganese Oxide Ion Sieve MnO2·0.5H2O." Colloids and Surfaces A: Physicochemical and Engineering Aspects 468: 280–84. https://doi.org/10.1016/j.colsurfa.2014.12.025.

Liu, Qi Xia, Yi Ru Zhou, Mei Wang, Qian Zhang, Tao Ji, Tian Ye Chen, and De Cheng Yu. 2019. "Adsorption of Methylene Blue from Aqueous Solution onto Viscose-Based Activated Carbon Fiber Felts: Kinetics and Equilibrium Studies." Adsorption Science and Technology 37 (3–4): 312–32. https://doi.org/10.1177/0263617419827437.

Liu, Yu, Hui Xu, Shu Fang Yang, and Joo Hwa Tay. 2003. "A General Model for Biosorption of Cd2+, Cu2+ and Zn2+ by Aerobic Granules." Journal of Biotechnology 102 (3): 233–39. https://doi.org/10.1016/S0168-1656(03)00030-0.

Messa, Lucas Luiz, Roselena Faez, and You-Lo Hsieh. 2021. "Phosphorylated Cellulose Nanofibrils from Sugarcane Bagasse with PH Tunable Gelation." Carbohydrate Polymer Technologies and Applications 2 (April): 100085. https://doi.org/10.1016/j.carpta.2021.100085.

Murodjon, Samadiy, Xiaoping Yu, Mingli Li, Ji Duo, and Tianlong Deng. 2020. "Lithium Recovery from Brines Including Seawater, Salt Lake Brine, Underground Water and Geothermal Water." Thermodynamics and Energy Engineering, 1–39. https://doi.org/10.5772/intechopen.90371.

Nayaka, G. P., J. Manjanna, K. V. Pai, R. Vadavi, S. J. Keny, and V. S. Tripathi. 2015. "Recovery of Valuable Metal Ions from the Spent Lithium-Ion Battery Using Aqueous Mixture of Mild Organic Acids as Alternative to Mineral Acids." Hydrometallurgy 151: 73–77. https://doi.org/10.1016/j.hydromet.2014.11.006.

Ndi Nsami, Julius, and Joseph Ketcha Mbadcam. 2013. "The Adsorption Efficiency of Chemically Prepared Activated Carbon from Cola Nut Shells by ZnCl2 on Methylene Blue." Journal of Chemistry 2013. https://doi.org/10.1155/2013/469170.

Nidheesh, P. V., Abhijeet Kumar, D. Syam Babu, Jaimy Scaria, and M. Suresh Kumar. 2020. "Treatment of Mixed Industrial Wastewater by Electrocoagulation and Indirect Electrochemical Oxidation." Chemosphere 251: 126437. https://doi.org/10.1016/j.chemosphere.2020.126437.

Nishihama, Syouhei, Kenta Onishi, and Kazuharu Yoshizuka. 2011. "Selective Recovery Process of Lithium from Seawater Using Integrated Ion Exchange Methods." Solvent Extraction and Ion Exchange 29 (3): 421–31. https://doi.org/10.1080/07366299.2011.573435.

Olawale, Salaudeen Abdulwasiu. 2020. "Biosorption of Heavy Metals from Aqueous Solutions:Insight and Review." Archives of Industrial Engineering 3 (October): 1–31. https://doi.org/10.31829/2637-9252/aie2020-3(1)-113.

Oliviera, Glaucia A C de, José O V Bustillos, João C Ferreira, Vanderlei S Bergamaschi, Rafaeli M de Moraes, Maíse P Gimenez, Flavia K Miyamoto, and José A Seneda. 2017. "Applications of Lithium in Nuclear Energy." INAC 2017: International Nuclear Atlantic Conference, 2–6. http://inis.iaea.org/search/search.aspx?orig_q=RN:49018089.

Oruch, Ramadhan, Mahmoud A. Elderbi, Hassan A. Khattab, Ian F. Pryme, and Anders Lund. 2014. "Lithium: A Review of Pharmacology, Clinical Uses, and Toxicity." European Journal of Pharmacology 740 (June): 464–73. https://doi.org/10.1016/j.ejphar.2014.06.042.

Ouazzane, H., F. Laajine, M. El Yamani, J. El Hilaly, Y. Rharrabti, M. Y. Amarouch, and D. Mazouzi. 2017. "Olive Mill Solid Waste Characterization and Recycling Opportunities: A Review." Journal of Materials and Environmental Science 8 (8): 2632–50.

Pacheco, Claudia Marcela, Cecilia Bustos, Guillermo Reyes, María Graciela Aguayo, and Orlando J. Rojas. 2018. "Characterization of Residues from Chilean Blueberry Bushes: A Potential Source of Cellulose." BioResources 13 (4): 7345–59. https://doi.org/10.15376/BIORES.13.4.7345-7359.

Paliulis, Dainius. 2016. "Removal of Formaldehyde from Synthetic Wastewater Using Natural and Modified Zeolites." Polish Journal of Environmental Studies 25 (1): 251–57. https://doi.org/10.15244/pjoes/60727.

Papaoikonomou, Lygeri, Konstantinos Labanaris, Kyriakos Kaderides, and Athanasia M. Goula. 2021. "Adsorption–Desorption of Phenolic Compounds from Olive Mill Wastewater Using a Novel Low-Cost Biosorbent." Environmental Science and Pollution Research 28 (19): 24230–44. https://doi.org/10.1007/s11356-019-07277-2.

Pinna, Eliana G., M. C. Ruiz, Manuel W. Ojeda, and Mario H. Rodriguez. 2017. "Cathodes of Spent Li-Ion Batteries: Dissolution with Phosphoric Acid and Recovery of Lithium and Cobalt from Leach Liquors." Hydrometallurgy 167 (October 2016): 66–71. https://doi.org/10.1016/j.hydromet.2016.10.024.

Quek, S. Y., D. A.J. Wase, and C. F. Forster. 1998. "The Use of Sago Waste for the Sorption of Lead and Copper." Water SA 24 (3): 251–56.

Rahimi Kord Sofla, M., R. J. Brown, T. Tsuzuki, and T. J. Rainey. 2016. "A Comparison of Cellulose Nanocrystals and Cellulose Nanofibres Extracted from Bagasse Using Acid and Ball Milling Methods." Advances in Natural Sciences: Nanoscience and Nanotechnology 7 (3). https://doi.org/10.1088/2043-6262/7/3/035004.

Recepoğlu, Yaşar K., Nalan Kabay, İdil Yılmaz-Ipek, Müşerref Arda, Kazuharu Yoshizuka, Syouhei Nishihama, and Mithat Yüksel. 2017. "Equilibrium and Kinetic Studies on Lithium Adsorption from Geothermal Water by λ-MnO2." Solvent Extraction and Ion Exchange 35 (3): 221–31. https://doi.org/10.1080/07366299.2017.1319235.

Recepoğlu, Yaşar Kemal, and Asli Yüksel. 2021a. "Synthesis, Characterization and Adsorption Studies of Phosphorylated Cellulose for the Recovery of Lithium from Aqueous Solutions." Cellulose Chemistry and Technology 55 (3–4): 385–401. https://doi.org/10.35812/CELLULOSECHEMTECHNOL.2021.55.37.

Recepoğlu, Yaşar Kemal, and Aslı Yüksel. 2021b. "Phosphorylated Hazelnut Shell Waste for Sustainable Lithium Recovery Application as Biosorbent." Cellulose 3. https://doi.org/10.1007/s10570-021-04148-3.

Riaz, Muhammad, Raziya Nadeem, Muhammad Asif Hanif, Tariq Mehmood Ansari, and Khalil ur Rehman. 2009. "Pb(II) Biosorption from Hazardous Aqueous Streams Using Gossypium Hirsutum (Cotton) Waste Biomass." Journal of Hazardous Materials 161 (1): 88–94. https://doi.org/10.1016/j.jhazmat.2008.03.096.

Rol, Fleur, Cécile Sillard, Michel Bardet, Jayasubba Reddy Yarava, Lyndon Emsley, Corinne Gablin, Didier Léonard, Naceur Belgacem, and Julien Bras. 2020. "Cellulose Phosphorylation Comparison and Analysis of Phosphorate Position on Cellulose Fibers." Carbohydrate Polymers 229 (September 2019): 115294. https://doi.org/10.1016/j.carbpol.2019.115294.

Rona, M., and G. Schmuckler. 1973. "Separation of Lithium from Dead Sea Brines by Gel Permeation Chromatography." Talanta 20 (2): 237–40. https://doi.org/10.1016/0039-9140(73)80275-9.

Ryu, Taegong, Junho Shin, Dong Hee Lee, Jungho Ryu, Insu Park, Hyejin Hong, Byoung Gyu Kim, Jin Bae Lee, Yun Suk Huh, and Kang Sup Chung. 2015. "Improvement of Lithium Adsorption Capacity of Porous Cylinder-Type Lithium Manganese Oxide through Introduction of Additive." Materials Chemistry and Physics 167: 225–30. https://doi.org/10.1016/j.matchemphys.2015.10.036.

Saha, Tapan Kumar. 2010. "Adsorption of Methyl Orange onto Chitosan from Aqueous Solution." Journal of Water Resource and Protection 02 (10): 898–906. https://doi.org/10.4236/jwarp.2010.210107.

Sari, Ahmet, Durali Mendil, Mustafa Tuzen, and Mustafa Soylak. 2008. "Biosorption of Cd(II) and Cr(III) from Aqueous Solution by Moss (Hylocomium Splendens) Biomass: Equilibrium, Kinetic and Thermodynamic Studies." Chemical Engineering Journal 144 (1): 1–9. https://doi.org/10.1016/j.cej.2007.12.020.

Sarker, Tushar C., Shah Md Golam Gousul Azam, Ahmed M.Abd El-Gawad, Salvatore A. Gaglione, and Giuliano Bonanomi. 2017. "Sugarcane Bagasse: A Potential Low-Cost Biosorbent for the Removal of Hazardous Materials." Clean Technologies and Environmental Policy 19 (10): 2343–62. https://doi.org/10.1007/s10098-017-1429-7.

Sekhararao Gulipalli, Ch, B. Prasad, and Kailas L. Wasewar. 2011. "Batch Study, Equilibirum and Kinetics of Adsorption of Selenium Using Rice Husk Ash (RHA)." Journal of Engineering Science and Technology 6 (5): 590–609.

Shi, Chenglong, Yan Jing, Jiang Xiao, Xingquan Wang, Ying Yao, and Yongzhong Jia. 2017. "Solvent Extraction of Lithium from Aqueous Solution Using Non-Fluorinated Functionalized Ionic Liquids as Extraction Agents." Separation and Purification Technology 172: 473–79. https://doi.org/10.1016/j.seppur.2016.08.034.

Singh, Raj P., and Nureddin M. Abbas. 1996. "Suppressed Ion Chromatographic Determination of Lithium, Sodium, Ammonium and Potassium Concentrations in Sub-Surface Brines." Journal of Chromatography A 733 (1–2): 93–99. https://doi.org/10.1016/0021-9673(95)00958-2.

Sousa, Francisco W., André G. Oliveira, Jefferson P. Ribeiro, Morsyleide F. Rosa, Denis Keukeleire, and Ronaldo F. Nascimento. 2010. "Green Coconut Shells Applied as Adsorbent for Removal of Toxic Metal Ions Using Fixed-Bed Column Technology." Journal of Environmental Management 91 (8): 1634–40. https://doi.org/10.1016/j.jenvman.2010.02.011.

Suflet, Dana Mihaela, Gabrielle Charlotte Chitanu, and Valentin I. Popa. 2006. "Phosphorylation of Polysaccharides: New Results on Synthesis and Characterisation of Phosphorylated Cellulose." Reactive and Functional Polymers 66 (11): 1240–49. https://doi.org/10.1016/j.reactfunctpolym.2006.03.006.

Tirtom, Vedia Nüket, Ayşe Dinçer, Seda Becerik, Tülin Aydemir, and Ali Çelik. 2012. "Removal of Lead (II) Ions from Aqueous Solution by Using Crosslinked Chitosan-Clay Beads." Desalination and Water Treatment 39 (1–3): 76–82. https://doi.org/10.1080/19443994.2012.669161.

Tzanov, Tzanko, Maria Stamenova, and Artur Cavaco-Paulo. 2002. "Phosphorylation of Cotton Cellulose with Baker's Yeast Hexokinase." Macromolecular Rapid Communications 23 (16): 962–64. https://doi.org/10.1002/1521-3927(200211)23:16<962::AID-MARC962>3.0.CO;2-B.

Um, Namil, and Tetsuji Hirato. 2014. "Precipitation Behavior of Ca(OH)2, Mg(OH)2, and Mn(OH)2 from CaCl2, MgCl2, and MnCl2 in NaOH-H2O Solutions and Study of Lithium Recovery from Seawater via Two-Stage Precipitation Process." Hydrometallurgy 146: 142–48. https://doi.org/10.1016/j.hydromet.2014.04.006.

Verduzco-Navarro, Ilse Paulina, Nely Rios-Donato, Carlos Federico Jasso-Gastinel, Álvaro de Jesús Martínez-Gómez, and Eduardo Mendizábal. 2020. "Removal of Cu(II) by Fixed-Bed Columns Using Alg-Ch and Alg-Chs Hydrogel Beads: Effect of Operating Conditions on the Mass Transfer Zone." Polymers 12 (10): 1–18. https://doi.org/10.3390/polym12102345.

Vieira, M. G.A., A. F. De Almeida Neto, M. G.C. Da Silva, C. N. Carneiro, and A. A.Melo Filho. 2014. "Adsorption of Lead and Copper Ions from Aqueous Effluents on Rice Husk Ash in a Dynamic System." Brazilian Journal of Chemical Engineering 31 (2): 519–29. https://doi.org/10.1590/0104-6632.20140312s00002103.

Vizárová, Katarína, Soňa Kirschnerová, František Kačík, Anna Briškárová, Štefan Šutý, and Svetozár Katuščák. 2012. "Relationship between the Decrease of Degree of Polymerisation of Cellulose and the Loss of Groundwood Pulp Paper Mechanical Properties during Accelerated Ageing." Chemical Papers 66 (12): 1124–29. https://doi.org/10.2478/s11696-012-0236-1.

Wahib, Sara A., Dana A. Da'na, Nabil Zaouri, Yousef M. Hijji, and Mohammad A. Al-Ghouti. 2022. "Adsorption and Recovery of Lithium Ions from Groundwater Using Date Pits Impregnated with Cellulose Nanocrystals and Ionic Liquid." Journal of Hazardous Materials 421 (July 2021): 126657. https://doi.org/10.1016/j.jhazmat.2021.126657.

Wang, Shulei, Xin Chen, Ying Zhang, Yang Zhang, and Shili Zheng. 2018. "Lithium Adsorption from Brine by Iron-Doped Titanium Lithium Ion Sieves." Particuology 41: 40–47. https://doi.org/10.1016/j.partic.2018.02.001.

Xu, Chenxi, Tianlin Yu, Jing Peng, Long Zhao, Jiuqiang Li, and Maolin Zhai. 2020. "Efficient Adsorption Performance of Lithium Ion onto Cellulose Microspheres with Sulfonic Acid Groups." Quantum Beam Science 4 (1): 6. https://doi.org/10.3390/qubs4010006.

Xu, Hui, and Donghong Guo. 2012. "Synthesis and Characterization of an Ion-Imprinted Polymer for Selective Adsorption of Copper Ions in Aqueous Solution." Adsorption Science and Technology 30 (4): 293–306. https://doi.org/10.1260/0263-6174.30.4.293.

Xu, Xin, Yongmei Chen, Pingyu Wan, Khaled Gasem, Kaiying Wang, Ting He, Hertanto Adidharma, and Maohong Fan. 2016. "Extraction of Lithium with Functionalized Lithium Ion-Sieves." Progress in Materials Science 84: 276–313. https://doi.org/10.1016/j.pmatsci.2016.09.004.

Yu, Zhen, Shaoan Cheng, Ruonan Gu, Yihang Li, Shaoling Dai, and Zhengzhong Mao. 2021. "Interfacial Solar Evaporator for Clean Water Production and beyond: From Design to Application." Applied Energy 299 (June): 117317. https://doi.org/10.1016/j.apenergy.2021.117317.

Yuan, Caideng, Lei Zhang, Haichao Li, Ruiwei Guo, Meng Zhao, and Lan Yang. 2019. "Highly Selective Lithium Ion Adsorbents: Polymeric Porous Microsphere with Crown Ether Groups." Transactions of Tianjin University 25 (2): 101–9. https://doi.org/10.1007/s12209-018-0147-5.

Zandevakili, Saeed, Mohammad Ranjbar, and Maryam Ehteshamzadeh. 2014. "Synthesis of Lithium Ion Sieve Nanoparticles and Optimizing Uptake Capacity by Taguchi Method." Iranian Journal of Chemistry and Chemical Engineering 33 (4): 15–24.

Zante, Guillaume, Maria Boltoeva, Abderrazak Masmoudi, Rémi Barillon, and Dominique Trébouet. 2019. "Lithium Extraction from Complex Aqueous Solutions Using Supported Ionic Liquid Membranes." Journal of Membrane Science 580: 62–76. https://doi.org/10.1016/j.memsci.2019.03.013.

Zhang, Helan. 2014. "Biosorption of Heavy Metals from Aqueous Solutions Using Keratin Biomaterials."

Zhang, Qi, Yingshi Zhang, Yu Shen, Qing Ye, Qilin Cai, and Xi Wu. 2021. "Improving Seawater Desalination Efficiency by Solar Driven Interfacial Evaporation Based on Biochar Evaporator of Nannochloropsis Oculata Residue." Journal of Environmental Chemical Engineering 9 (4). https://doi.org/10.1016/j.jece.2021.105787.

Zhao, Chunlong, Mingming He, Hongbin Cao, Xiaohong Zheng, Wenfang Gao, Yong Sun, He Zhao, Dalong Liu, Yanling Zhang, and Zhi Sun. 2020. "Investigation of Solution Chemistry to Enable Efficient Lithium Recovery from Low-Concentration Lithium-Containing Wastewater." Frontiers of Chemical Science and Engineering 14 (4): 639–50. https://doi.org/10.1007/s11705-019-1806-3.

Zhou, Yanmei, and Min Zhang. 2016. "Response to 'Comment on "Removal of Crystal Violet by a Novel Cellulose-Based Adsorbent: Comparison with Native Cellulose."'" Industrial and Engineering Chemistry Research 55 (4): 1148. https://doi.org/10.1021/acs.iecr.5b04874.

Zhou, Zhiyong, Wei Qin, Yang Liu, and Weiyang Fei. 2012. "Extraction Equilibria of Lithium with Tributyl Phosphate in Kerosene and FeCl 3." Journal of Chemical and Engineering Data 57 (1): 82–86. https://doi.org/10.1021/je200803h.
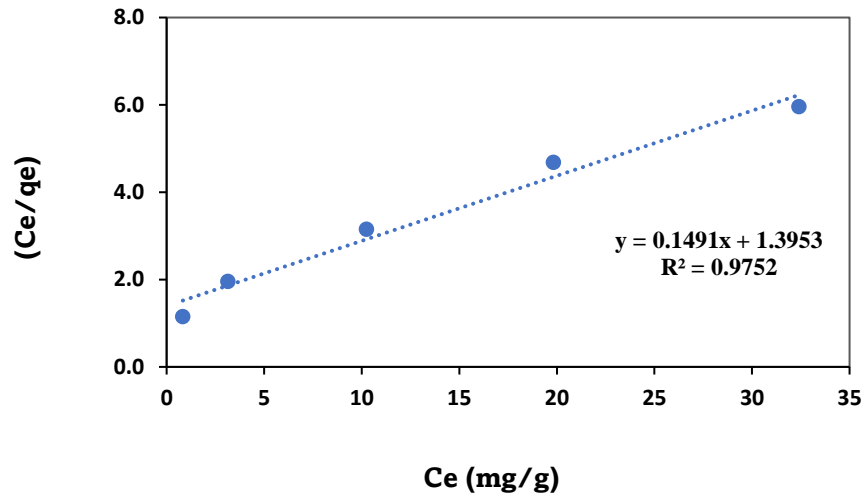
APPENDIX A

LANGMUIR MODEL CURVES

y = 0.1491x + 1.3953
R² = 0.9752

Figure A1. Langmuir model curve of FOB (T=30◦C, Co=10-100mg/L)

y = 0.1509x + 1.5241
R² = 0.9752
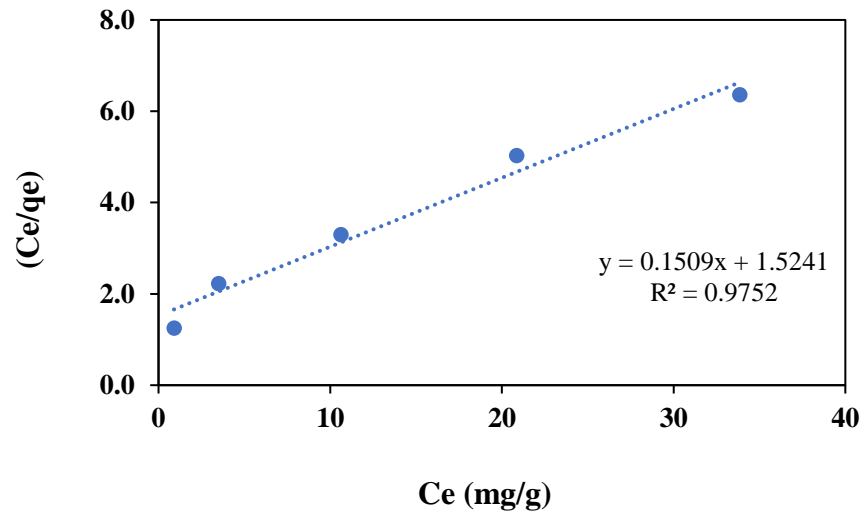
Figure A2. Langmuir model curve of FOB (T=40◦C, Co=10-100mg/L)
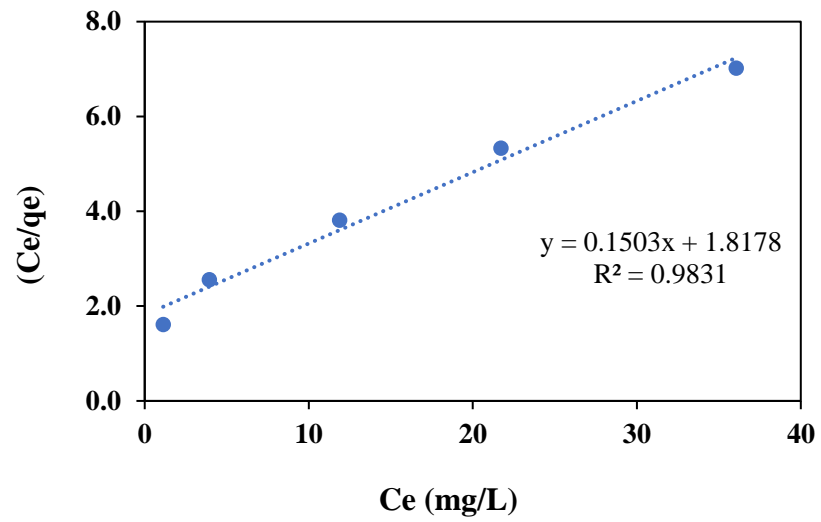
Figure A3. Langmuir model curve of FOB (T=50◦C, Co=10-100mg/L)

APPENDIX B

FREUNDLICH MODEL CURVES
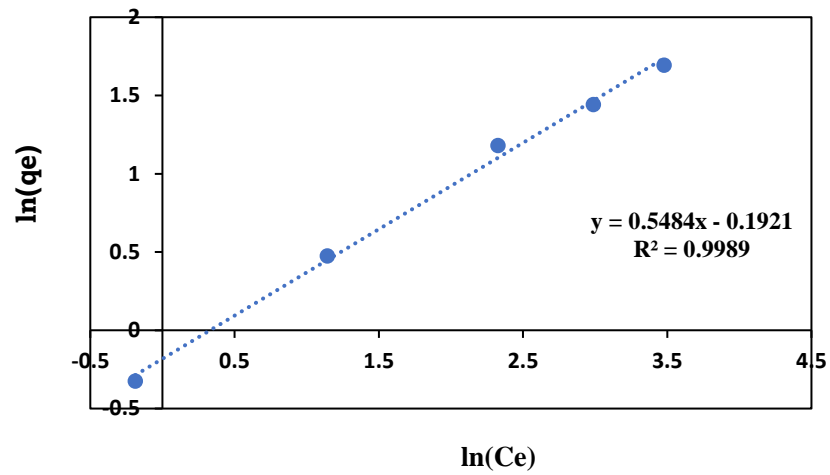
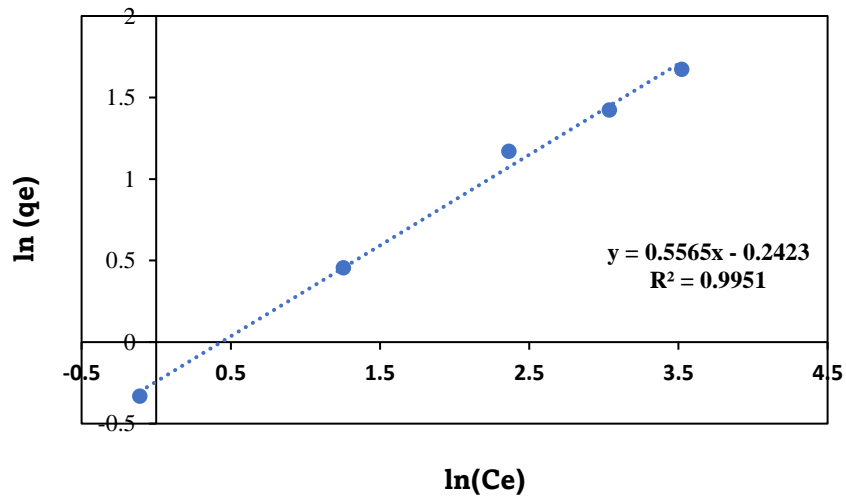**Figure B1.** Freundlich model curve of FOB at 30 ˚C,
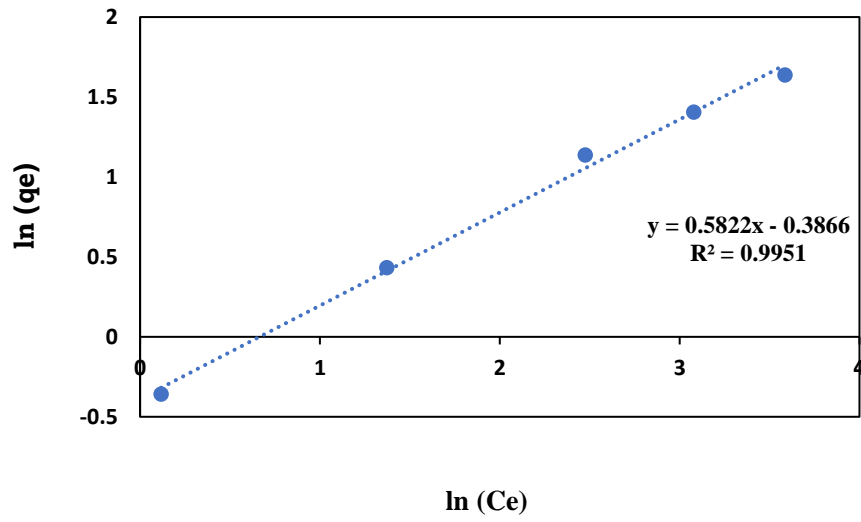

Figure B2. Freundlich model curve of FOB at 40 ˚C

Figure B3. Freundlich model curve of FOB at 50 °C